Neural circuits for long-range color filling-in

Peggy Gerardin[1], Clément Abbatecola[1], Frédéric Devinck[2], Henry Kennedy[1], Michel Dojat[3], Kenneth Knoblauch[1]

[1] Univ Lyon, Université Claude Bernard Lyon 1, Inserm, Stem Cell and Brain Research Institute U1208, 69500 Bron, France.

[2] Université Rennes 2, CRPCC, EA 1285, 35000 Rennes, France

[3] Univ. Grenoble Alpes, Inserm, CHU Grenoble Alpes, GIN, 38000 Grenoble, France

Running Title: Neural correlates of filling-in.

Correspondence should be addressed to: Peggy Gerardin & Kenneth Knoblauch, INSERM U1208 Stem-Cell and Brain Research Institute, 69500 Bron, France.

Email: peggy.gerardin@inserm.fr, ken.knoblauch@inserm.fr

Keywords: Functional MRI, Surface Color Appearance, Human Vision, Functional Streams, Cortical Hierarchy

Abstract

Surface color appearance depends on both local surface chromaticity and global context. Understanding these inter-dependencies provides insight into the network properties of the visual system. Combining functional imaging and psychophysics, we ask whether color from long-range filling-in and from a matched region of uniform chromaticity engage common pathways. We find that color from filling-in is best classified and best correlated with appearance by two dorsal areas, V3A and V3B/KO. In contrast, a uniform chromaticity is best classified by ventral areas hV4 and LO. Dynamic causal modeling revealed feedback modulation from area LO to areas V1 and V3A for uniform color surfaces, contrasting with feedback from V3A modulating areas V1 and LO for filling-in. These results indicate a dorsal stream role in color filling-in via feedback modulation of area V1 coupled with a cross-stream modulation of ventral areas suggesting that local and distant influences on color appearance engage distinct neural networks.

Introduction

Surface color appearance depends on multiple factors. In the absence of contextual information, color appearance largely depends on surface spectral information and will be referred to as *surface-dependent color*. Nevertheless, contextual features influence and modulate color appearance. Surface color perception that is driven by remote contours is referred to as filling-in. Long-range filling-in phenomena suggest that the color appearance of surfaces depends on combining local surface information with contextual information, such as from distant edges. We will refer to the latter as *edge-dependent or induced* color. The contributions of contextual influences to surface color appearance have interested scientists for many years and have been successfully studied via a number of visual phenomena, including simultaneous contrast (Chevreul 1839), neon-color spreading (Varin 1971), and, more recently by the Watercolor Effect (Pinna, Brelstaff, and Spillmann 2001). In contrast to the progress made on the psychophysics of these phenomena, little is known about the distributed neural representation of edge-induced filling-in percepts and to what extent identical percepts induced by edge and surface information depend on common or distinct neural networks.

A common hypothesis is that surface- and edge-dependent percepts generate equivalent neural activity at early visual stages (Komatsu 2006). Ratliff and Sirovich (1978) noted that convolution with center-surround like filters both of step-edges and of the spatial transients that induce filling-in (e.g., Craik-O'Brien-Cornsweet effects) results in nearly identical images (Figure 1). One hypothesis is that the center-surround receptive field organization in early vision could lead to edge transients and surfaces generating equivalent neural response profiles that the observer would perceive similarly. Bayesian models of perception predict that both such stimuli would be perceived as uniform fields because they would correspond to the most likely cause of the neural activation (Brown and Friston 2012). This proposal is agnostic, however, with respect to whether the underlying neural representations generate retinotopically-distributed activity isomorphic with the fill-in percept at a subsequent stage (Anstis 2010). Such a proposal is compatible with reports that in cortical area V1 the most frequently encountered color sensitive cells are double-opponent that respond best to isolated chromatic contours but also to the edges of uniform color and luminance surfaces (Friedman, Zhou, and von der Heydt 2003, Johnson, Hawken, and Shapley 2001). These cells show response profiles that are stronger for stimulus edges than uniform surfaces (Friedman, Zhou, and von der

61 Heydt 2003), and, in fact, optical imaging experiments using voltage sensitive dyes in macaque (Zweig
62 et al. 2015) and functional imaging in humans (Cornelissen et al. 2006) demonstrate that the response
63 profiles in area V1 for uniform luminance or chromatic surfaces are dominated by edge responses.

64 In area V1, it is conceivable that surface- and edge-dependent percepts could be processed
65 through distinct neural channels. Double-opponent cells in area V1 could carry information about both
66 isolated chromatic and luminance edge-transients, such as those that generate filling-in, as well as the
67 edges of uniform surfaces while single-opponent cells would respond optimally to the interior region of
68 uniform fields. Signal-opponent receptive fields display different spectral sensitivities in spatially
69 distinct excitatory and inhibitory regions, thereby giving rise to spectrally dependent responses to
70 uniform fields. Such an organization would be consistent with theories of visual processing that
71 propose independent surface and edge processing in form perception (Pinna and Grossberg 2005).
72 While the population of single opponent cells in V1 is estimated to be less than half that of the double-
73 opponent cells, this may simply reflect differences in the sampling requirements for detecting uniform
74 surfaces and edges (Schluppeck and Engel 2002). In higher visual areas little is known about the
75 relative contribution of edge-dependent and local surface processing mechanisms. Here, we ask
76 whether or not the neural activity resulting from edge-induced color filling-in of a surface is channeled
77 through the same cortical inter-areal networks as the activity generated by a surface of matched
78 uniform chromaticity?

79 The edge-induced, filling-in phenomenon known as the Watercolor Effect (WCE) is ideal for
80 evaluating these two hypotheses (Figure 2a). In the WCE, the color of the inner contour of a pair of
81 distant, chromatic contours modifies the appearance of an interior region that is physically identical to
82 the background in such a manner that it appears as a uniform, desaturated hue (Pinna, Brelstaff, and
83 Spillmann 2001). The WCE propagates over too large a visual angle to be attributed to light spread in
84 the eye. However, to date, investigation of the WCE has provided little evidence concerning the
85 neuronal underpinnings of the phenomena. Importantly, based on theoretical and psychophysical
86 observations (Devinck et al. 2014), the thin chromatic edge-transient that induces the WCE is
87 expected to preferentially activate edge-sensitive double opponent cells in area V1 rather than surface
88 responsive single opponent cells. While Coia et al. (2014) obtained evidence from the visual evoked
89 potential (VEP) correlates with psychophysical responses for the WCE, insufficient resolution of the
90 VEP make it impossible to localize the areas implicated in the processing. Finally, both the large

extent of the filling-in and the sensitivity of the phenomenon to the curvature of the inducing contours (Gerardin et al. 2014) point to the involvement of cortical areas beyond V1 and V2.

Here, we used functional magnetic resonance imaging (fMRI) combined with Multi-Voxel Pattern Analysis (MVPA) in order to localize those cortical areas associated with edge-induced, color filling-in of the WCE phenomenon and those responding to a matched uniform chromaticity. To validate the functional imaging findings, we compared the blood oxygen-level dependent (BOLD) signal with the psychophysically estimated strength of the WCE. The MVPA results demonstrate that neural activity supporting the WCE is distributed across multiple hierarchical levels and streams in the visual system, but only a small set of higher order dorsal areas are related to the perceptual strength of the phenomenon. Combining Dynamic Causal Modeling (DCM) with Bayesian Model Selection, shows that the areas most associated with the WCE exhibit a feedback modulation on area V1 and the ventral stream, and the directions of these modulations are reversed for the matched uniform chromaticity. The results suggest that the WCE color filling-in depends, at least in part, on a dorsal stream influence on ventral color areas. They support the idea that edge-induced filling-in and surface-dependent color are processed through distinct networks across the cortical hierarchy engaging ascending and descending pathways.

Results

Estimated perceived strength of WCE

Perceptual scales were estimated by Maximum Likelihood Difference Scaling (MLDS), method of triads (Knoblauch and Maloney 2008, Maloney and Yang 2003), a powerful method for identification of perceptual correlates of BOLD responses (Bellot et al. 2016, Yang, Szeverenyi, and Ts'o 2008). A sample trial illustrating the stimulus configuration is shown in Figure 3a. The approach is based on the idea that when the perceived filling-in of the upper stimulus is judged equally often to be as similar to the lower left as to the lower right stimulus, then the perceived differences between a and b and between b and c are equal. This allows scale values to be estimated by maximum likelihood based on a signal detection model of the observer decision rule (Knoblauch and Maloney 2012, Maloney and Yang 2003). Individual (left panel) and average (right panel) perceptual scales estimated by MLDS

121 (Figure 3b) display the dependence of the strength of the filling-in on the luminance of the orange
122 contour for test (filled circles) and control (open circles) stimuli. With test stimuli the filling-in response
123 increases with the elevation of the luminance of the interior contour with respect to an equiluminant
124 plane in DKL space, while for the control stimuli responses are attenuated or absent (Devinck et al.
125 2014, Devinck and Knoblauch 2012). The differences in response magnitude between edge-
126 dependent and braided control stimuli confirms that observers respond to the fill-in color and not the
127 contours, and reveals significant differences in the strength of the WCE across observers. Figure 3c
128 shows for all observers two scatterplots of the luminance elevation that best match the WCE against
129 the peak MLDS response for the edge-dependent stimulus (left panel) and the control stimulus (right
130 panel). As the luminance elevation of the matched stimulus decreases in DKL space, colorimetric
131 purity increases. Thus, lower luminance matches correspond to a higher matched colorimetric purity
132 and therefore, a stronger perceived fill-in color in the edge-dependent stimulus. The strength of the
133 WCE is significantly correlated with the matched color value ($r=-0.62$, $p=0.01$) for the edge-dependent
134 but not for the control stimulus ($r = -0.19$, $p = 0.48$). Thus, individual differences in the strength of the
135 WCE covary similarly for both the scaling and matching data.
136
137 **Rationale of test and control conditions for imaging experiments**
138 Table 1 shows the pattern of feature differences among the three stimulus conditions that we used
139 and on the basis of which we can make comparisons and inferences about the role of particular
140 Regions of Interest (ROIs) on edge and surface dependent color appearance. Because each
141 comparison varies for two features, no comparison uniquely defines the information treated by a ROI,
142 instead the interpretation of the source of the activation is constrained by the combined classification
143 across all three comparisons. For example, significant differences for the edge-dependent vs. control
144 comparison could result from either the local difference in edge continuity of the inducer or from the
145 difference in perceived color of the interior region. However, if the same ROI only weakly
146 differentiates the surface-dependent vs. edge-dependent, then the influence of the edge continuity on
147 the response can be excluded since these stimuli also differ with respect to that feature. In this case,
148 we infer that the area's response is implicated in the treatment of filling-in. If in addition the ROI
149 weakly differentiates surface vs. control conditions, then it implies that the ROI's response does not
150 depend strongly on the surface chromaticity since that feature is a common feature to the two

comparisons showing weak classification. On the other hand, if an ROI strongly responds to both the edge-dependent vs. surface and the surface vs. control conditions but not the edge-dependent vs. control, then we can conclude that it responds on the basis of a purely stimulus bound feature, the interior chromaticity difference, since that is the only common feature.

BOLD activation related to the WCE

A whole-brain analysis using a General Linear Model (GLM) was undertaken so as to detect significant BOLD activation related to the WCE. With this aim, stimulus blocks from each of the three conditions were contrasted with the other two in a group analysis. No significant activation was revealed ($p>0.05$, Bonferroni corrected for all brain voxels).

Discriminating edge-dependent and surface-dependent processing with MVPA

To obtain a more fine-grained analysis of the contrasts, MVPA was applied to ROIs identified by functional localizers. We assumed that if a ROI is involved in edge- or surface-dependent color appearance, contrasts in the stimuli would generate a significantly higher accuracy than chance according to the logic expressed above and with respect to Table 1. Signal-to-noise ratios tested by a linear mixed-effects model across cortical areas and with a random observer intercept showed no significant differences that would bias such comparisons (Likelihood ratio test: $\chi^2(9) = 7.4; p = 0.6$, Figure S1).

MVPA was used to test how activity patterns of voxels in retinotopic areas (V1, V2), dorsal areas (V3d, V3A, V7, V3B/KO, hMT+/V5) and ventral areas (V3v, hV4, LO), are sensitive to the WCE. As demonstrated previously (Devinck et al. 2014, Gerardin et al. 2014) and confirmed in the psychophysical experiments above, WCE filling-in is absent or strongly attenuated when the stimulus contour is braided. Classifiers were run to identify regions that respond preferentially to these particular properties of the edge-dependent stimuli (WCE). Analyses were also conducted to reveal visual regions that respond to the processing of the surface-dependent stimuli matched in color appearance to the WCE. For each area, three classifiers tested specific hypotheses: (I) that accuracy was higher for the classification of edge-dependent than control stimuli; (II) that accuracy was higher for the classification of surface-dependent than control stimuli and (III) that accuracy was higher for the classification of edge- than. the surface-dependent color stimuli. All results reported below were

corrected for multiple testing (Holm 1979).

The 95% confidence intervals of the classification accuracies for all of the non-shuffled conditions (Figure 4, left bar in each of the three pairs in each graph and Table S1) exclude chance level at 50% while those for the shuffled control analyses (Figure 4, right bar in each pair) all include chance. These results suggest that processing of the stimuli tested is distributed across many areas. However, not all areas responded differentially to the three classifiers. For 4 areas (V2, V3d, V7 and hMT+/V5), the classification accuracies showed no selectivity for the conditions (Table S2, linear mixed effects model: V2: $F(2, 30) = 2.96$, $p = 0.07$; V3d: $F(2, 30) = 0.87$ $p = 0.42$; V7: $F(2, 30) = 1.53$, $p = 0.23$; hMT+/V5: $F(2, 30) = 0.28$, $p = 0.76$), and except for area V2, which classified robustly for all three MVPA rules, displayed relatively low prediction accuracies. Significant differences between the MVPA rules were observed in V1 (Table S2, linear mixed-effects model: $F(2,30)=16.58$, $p<0.001$) and in ventral stream areas (V3v: $F(2,30)=7.61$, $p<0.01$); hV4: $F(2,30)=11.78$, $p<0.001$; LO: $F(2,30)=17.14$, $p<0.0001$). In dorsal areas, differences between the MVPA rules only attained significance for areas V3A ($F(2,30)=47.05$, $p<0.00001$) and V3B/KO ($F(2,30)=27.27$, $p<0.00001$) (Table S2).

In independent sessions, the measures were repeated in three of the observers using stimuli of 4 deg diameter. The average of their results are indicated by the yellow points. In general, they replicate the same patterns as for the larger stimuli and support the robustness of the findings.

Ventral and dorsal stream areas systematically differ according to the patterns of classification accuracy across the three MVPA rules. Ventral areas (V3v, hV4 and LO) displayed higher accuracies for the surface-dependent vs. edge-dependent classifier that additionally were significantly greater than for the edge-dependent vs. control rule (Table 2, Tukey test, V3v: $t(885) = -4.3$, $p < 0.001$; hV4: $t(885) = -2.5$, $p < 0.05$; LO: $t(885) = -5.2$, $p < 0.001$). If the classifiers were driven by the edge continuity, then both rules would be expected to indicate high prediction accuracy. Instead, the results suggest that the classifications depended on the interior chromaticity of the stimuli, an interpretation reinforced by the high accuracy of the surface-dependent vs. control comparison (significantly greater than the edge-dependent vs. control condition for areas V3v and hV4: Table 2, Tukey test, I vs II: V3v: $t(885) = -3.1$, $p < 0.01$ and hV4: $t(885) = -4.7$, $p < 0.001$) that differed in the interior chromaticity.

Dorsal stream areas (V3A and V3B/KO) showed a complementary pattern of results in which classification accuracy was highest for the edge-dependent vs. control condition and significantly higher than for the other two rules (Table 2, Tukey test, V3A, I vs. II: $t(885) = 6.50$; $p < 0.001$; I vs. III;

211 t(885) = 8.50, p < 0.001; V3B/KO: I vs. II: t(885) = 7.10, p < 0.001; I vs. III: t(885) = 7.30; p < 0.001).
212 The high accuracy in these areas for the edge-dependent vs. control rule supports either a
213 classification on the basis of the filling-in or the edge continuity. The surface-dependent vs. edge-
214 dependent comparison, however, also differed in edge continuity so that the significantly lower
215 response in this case argues in favor of filling-in and against a role for edge continuity. In addition, the
216 significantly lower response of the surface-dependent vs. control comparison argues against an
217 important role for surface chromaticity *per se* in the classification behavior of these areas.
218 Areas V1 and V2 showed a similar pattern of prediction accuracy for the three classifiers, with
219 higher response on the first two, edge-dependent vs. control and surface-dependent vs. control, but
220 only in area V1 do the differences between comparisons attain significance. This pattern is consistent
221 with processing of the fill-in color and the surface color since the responses are strongest whether the
222 edge or the surface is the source of the perceived color and weakest when this attribute is matched.
223 However, the strong activity for all three classifiers could indicate the presence of subpopulations that
224 respond differentially to all of the dimensions along which these stimuli differ.
225
226 **Relationship between behavior and neural processing of the WCE**
227 The MVPA analysis reveals candidate areas implicated in the processing of the WCE filling-in,
228 but does not necessarily indicate any relation to perception. To explore such a link, the Pearson
229 product-moment correlations were calculated between the individual classification accuracies for the
230 edge-dependent vs. control MVPA rule and the peak values for the estimated perceptual scales (d'
231 from the MLDS task). None of the other rules should be related to the perceptual strength of the WCE
232 and with one exception (area hMT+/V5, edge-dependent vs. surface: r = 0.52, p = 0.04), no significant
233 positive correlations were observed. Figure 5 shows the scatterplots of classification accuracy vs. d'
234 with regression lines for all ROIs with the correlations and significance levels under the hypothesis of
235 no correlation indicated in each figure. Of all the cortical areas studied, only areas V3A and V3B/KO
236 showed a significant positive correlation (V3A: r = 0.66, p = 0.006, 95% CI (0.237, 0.869); V3B/KO: r
237 = 0.5, p = 0.049, 95% CI (0.004, 0.794)).
238 The correlation for area V3v is near the criterion of significance used throughout (V3v: r = 0.47,
239 p = 0.064, 95% CI (-0.030, 0.785), and one can legitimately question whether its value differs
240 significantly from that observed for area V3B/KO (Nieuwenhuis, Forstmann, and Wagenmakers 2011).

241 An analysis of covariance to predict classification accuracy with respect to the covariate d' and the
242 factor Area indicated a significant interaction ($F(9, 140) = 2.21$, $p = 0.025$), demonstrating the
243 presence of at least one slope that differed significantly from 0. Inspection of the estimated
244 coefficients for each area revealed significant slopes for areas V3A ($t(140) = 2.81$, $p = 0.006$), V3B/KO
245 ($t(140) = 2.43$, $p = 0.02$) and V3v ($t(140) = 2.04$, $p = 0.04$). Post-hoc tests, however, showed that the
246 slopes of both areas V3A and V3B/KO differed significantly from that of V3v (Tukey Honest Significant
247 Differences test: V3v - V3A: $t(140) = -7.4$, $p < 0.0001$; V3v - V3B/KO: $t(140) = -4.81$, $p = 0.0002$)
248 while the slope difference between areas V3A and V3B/KO is at chance (V3A – V3B/KO: $t(140) =$
249 2.59, $p = 0.2305$).
250
251 **Effective connectivity for edge-induced and surface-dependent colors**
252 The above results suggest a role for dorsal areas, particularly area V3A, in the WCE color filling-in.
253 This is surprising because this area, and more generally, dorsal stream areas are little implicated in
254 color processing. We hypothesized that such a role could be mediated through the action of these
255 dorsal stream areas on the ventral stream, which has more typically been implicated in color
256 processing. To evaluate this hypothesis, we used Dynamic Causal Modeling (DCM, (Stephan et al.
257 2010, Friston, Harrison, and Penny 2003)) and Bayesian Model Selection (BMS) to test the context
258 dependent modulation among areas that showed differential responses to WCE and the uniform
259 added chromaticity. To increase the power of the analysis, we limited evaluation to a triple of areas
260 that included area V1, which represents the visual input at the cortical level, and two areas, V3A and
261 LO, which based on the MVPA analyses, displayed the strongest contrast in their classification profiles
262 with respect to edge-dependent and surface-dependent stimuli. We hypothesized that these areas
263 would be the most likely set of areas to differentiate between the two conditions. We considered
264 models that contrasted the directional modulation of effective connectivity between each pair of the
265 triple when compared with the braided control stimulus. We only tested models with unidirectional
266 modulation of connections between each pair of areas to further reduce the number of models and
267 because we were only interested in the strongest modulation of effective connectivity between area
268 pairs. We considered a space of 12 models (4 patterns of modulation of connectivity of area V1 to
269 V3A and LO times 3 possible relations between V3A and LO), representing plausible effective

connectivities between these two areas and V1 (Figure 6a). V1 was always connected to the two areas, but we also included the hypothesis that there was no modulation between V3A and LO.

The protected exceedance probabilities (PEP) for the 12 models for each of the two conditions are shown in the bar graphs of Figure 6b for the edge- (left panel) and surface-dependent (right panel) conditions. The Bayesian Omnibus Risk factors (BOR) for the PEP profiles rejected the hypothesis that the models are equiprobable, thus, indicating that at least one differed significantly from the others (BOR = 0.002 for both cases). For the number of observers in our study, PEP values above 0.5 (the disambiguation threshold) are considered strong evidence in favor of the model (Rigoux et al. 2014). Thus, the edge-dependent condition strongly supported model M08 (PEP = 0.82) in which feedback connections from area V3A influence areas V1 and LO, and a feedforward connection from V1 modulates LO. The surface-dependent condition, however, strongly supported model M11 (PEP = 0.68), which displays a complementary set of modulations, i.e., LO exerting a feedback modulation on V1 and V3A and V1 a feedforward modulation of area V3A.

In the analyses above, areas V3A and LO were selected based on the clear contrast in their stimulus classification profiles. Concomitantly, we should expect that pairs of areas for which the classification accuracy was low and for which the profiles did not distinguish among the stimuli would not show evidence supporting different models of effective connectivity for the edge- and surface-dependent conditions. As a control, we examined a model space for the triple V1-V3d-V7 (Figure S2a). Both V3d and V7 showed low classification accuracies ($p < 0.6$) and there were no significant differences among the three comparisons performed (Figure 4). In addition, for all three of these areas, the correlations between the prediction accuracy and appearance measures were not significant (Figure 5). The analysis rejected the hypothesis that models were equiprobable (BOR < 0.05 for both edge and surface conditions), but the model for which the evidence was strongest was the same (M11) for both conditions (Edge: PEP = 0.039; Surface: PEP = 1.4e-4) (Figure S2b).

Discussion

In the current study, we compared cortical activity related to color appearance generated by either edge-induced filling-in or a uniform surface chromaticity and found them to be associated with complementary patterns of activity in dorsal and ventral visual streams. Three lines of evidence

support these results. First, the MVPA technique showed a significantly different profile of classification performance for the edge-dependent vs surface dependent conditions in dorsal areas V3A and V3B/KO compared to ventral areas V3v, hV4 and LO. It is unlikely that differential deployment of attentional mechanisms could explain these results as attention was uniformly controlled in all fMRI experiments. Second, individual differences in the psychophysically measured strength of the WCE were significantly correlated only with the classification performance of the edge-dependent stimulus in dorsal areas V3A and V3B/KO. Finally, a DCM analysis showed that a model for which the data provided the strongest evidence was one in which the effective connectivity from dorsal area V3A modulated V1 and ventral area LO when the edge-dependent stimulus was compared with the control. In contrast, complementary modulations of LO onto V1 and V3A were found for the surface-dependent comparison with the control. Importantly, given that the whole brain GLM analyses failed to detect significant differences among the stimulus conditions, the results obtained depended critically on the sensitivity of the fine-grained MVPA (Sapountzis et al. 2010) and the DCM methods (Stephan et al. 2010, Friston, Harrison, and Penny 2003). Taken together, the results demonstrate that signals associated with edge- and surface-dependent information are not represented identically across visuals areas. The results support the hypothesis that information about surface-dependent and edge-induced colors is transmitted through distinct neural pathways.

The results do not rule out the participation of other areas in mediating edge- and surface-dependent color appearance. Indeed, the MVPA results reveal classification performance above chance in all visual areas, although they do not all significantly distinguish between the three conditions. For example, it would be interesting to extend the DCM analyses to include area V2 because of its implication in color processing (Roe and Ts'o 1999) and contour extraction (Lee and Nguyen 2001). This would entail examining a space of effective connections between four areas with an accompanying combinatorial increase in the number of possible models that would need to be tested. The larger number of models would dilute the power of such an analysis without, for example, evidence from the MVPA to constrain the analysis to a relevant subset of hypotheses.

Implication of cortical areas in edge- and surface dependent color processing. While area V3A has not typically been associated with color processing, activity dependent markers revealed a sparse population of cells responsive to chromatic stimuli (Tootell et al. 2004). In addition, Hadjikhani et al.

330 (1998) included V3A in a set of areas that generated greater responses to color than luminance
331 modulated stimuli. More recently, Castaldi, et al. (2013), reported that V3A responds to chromatic
332 spatial features. A source of its influence on color areas could arise from the recently described
333 Vertical Occipital Fasciculus (Takemura et al. 2015) that links ventral and dorsal stream areas.
334 Area V3A exhibits response selectivity to stimulus features that are characteristic of the WCE.
335 V3A has been shown to be selective for contour curvature (Caplovitz and Tse 2007), a characteristic
336 of the inducer contours that is necessary to enhance the WCE but not sufficient to generate it alone,
337 e.g., as shown by the braided control contours here and in previous work (Devinck et al. 2014,
338 Gerardin et al. 2014). Area V3A is also implicated in filling-in phenomena, in that it was reported to
339 show increases in activity during Troxler fading (Mendola et al. 2006). Similarly in macaque, area V3
340 has been implicated in filling-in phenomena (De Weerd et al. 1995). V3A also shows much larger
341 spatial summation than do nearby cortical areas (Press et al. 2001) as might be expected for an area
342 involved in filling-in over extended regions of the visual field. In fact, the large areas of the visual field
343 over which the WCE can extend require mechanisms that are effective in the peripheral visual field.
344 The implication of dorsal areas in large scale filling-in is consistent with the bias of peripheral visual
345 field projections in the dorsal stream (Kravitz et al. 2013).
346
347 Early studies that reported retinotopically distributed neural activity due to brightness and color
348 filling-in in area V1 (Sasaki and Watanabe 2004) have been disputed (Zweig et al. 2015, Cornelissen
349 et al. 2006). Using fMRI, Cornelissen et al. (2006) found that surround-induced responses in V1 did
350 not depend on surround intensity but instead could be attributed to an extended edge-response. This
351 is consistent with voltage-sensitive dye-imaging in macaque that shows only edge responses to
352 uniform fields of color and luminance in V1 (Zweig et al. 2015). Instead, V1 responses to contours
353 have been attributed to figural effects rather than brightness or color filling-in (Kok and de Lange 2014,
354 Cornelissen et al. 2006, Lee and Nguyen 2001). Interestingly, the WCE stimulus is reported to
355 demonstrate both a long-range color filling-in and a strong influence on figure-ground segregation
356 (Von der Heydt and Pierson 2006, Pinna, Brelstaff, and Spillmann 2001). However, the results from
357 area V1 are not likely to be explained uniquely by figure-ground processing. The classification results
358 from this area (Figure 4) were based only on the voxels interior to those activated by the retinotopic
359 positions of the contours (blue regions in Figure 7). The highest prediction accuracy for V1 significantly

360 differed from that for both of the other classification rules and pitted the surface-dependent stimulus
361 against the braided control, i.e., stimuli having the same braided contour. Instead, this supports that
362 classification depended on the interior chromaticity and/or the perceived color and not local or long-
363 range contour detection (Table 1). The poor correlation of the classification accuracies from this area
364 with the perceived strength of the filling-in color (Figure 5) would support the former of these two
365 interpretations.
366
367 Areas V3v, hV4 and LO displayed their highest classification accuracy to the surface
368 chromaticity of the stimulus and not to the edge-induced fill-in conditions. In line with this outcome,
369 the classification accuracies for these areas were not correlated with the strength of the perceived
370 filling-in color. These results are consistent with previous studies that have demonstrated strong
371 responses of these ventral stream areas to uniform surface colors (Brouwer and Heeger 2009, Parkes
372 et al. 2009, Bouvier, Cardinal, and Engel 2008, Bartels and Zeki 2000, Hadjikhani et al. 1998, Sakai et
373 al. 1995).
374
375 Area V2 presents a more complex pattern of results in that the classifiers trained for this area
376 showed high accuracy for all three conditions with no selectivity between comparisons. This pattern of
377 results is consistent with neurophysiological studies in primates that show diverse cell classes in area
378 V2 including both those responsive to uniform color fields (Peng and Van Essen 2005, Roe and Ts'o
379 1999) and others that might be involved in contour detection and color induction (Roe and Ts'o 1999).
380
381 **Role of double- and single-opponent cells.** The initial segregation of responses to uniform color
382 fields and edges in neural sub-populations occurs as early as area V1 and may reflect the differential
383 responses of single- and double-opponent cells. The differing involvement of the dorsal and ventral
384 streams in edge and surface color responses could mean that these two cells classes project
385 differentially to extra-striate cortical areas with the ventral stream areas being dominated by signals
386 from single-opponent cells and the dorsal areas receiving projections predominantly from double-
387 opponent cells.
388 Population responses to uniform color fields in area V1 are dominated by edge responses as
389 demonstrated by optical imaging with voltage sensitive dyes (Zweig et al. 2015). This result could

390 reflect that double-opponent cells are the most numerous color sensitive cell class in area V1 at the
391 eccentricity examined. The less numerous single-opponent cells would be expected to respond as well
392 to uniform fields. Thus, the typical cortical response signature in area V1 to a uniform color field could
393 be expected to be a pattern of activity across cells with both types of receptive field profile. Isolated
394 chromatic edges and edge transients, however, would be expected to generate a response profile
395 dominated by double opponent cells.

396 Why then do chromatic edge-transients, such as in the case of the WCE, suffice to generate the
397 appearance of a weakly colored field, filling-in the interior of a uniform region interior to the chromatic
398 contour? It is significant that the color filling-in requires continuity of the bi-chromatic contour as shown
399 here and elsewhere (Devinck and Knoblauch 2012) by the lack of effect for the braided control
400 stimulus. This suggests a mechanism by which the coherence along the contour is integrated across
401 a population of double-opponent cells' responses that we hypothesize would be mediated via paths
402 from V1 to V3A. Such an interpretation is supported by recent results indicating that adaptation to
403 chromatic contours weakens the WCE while having no influence on the appearance of a field of
404 uniform chromaticity (Coia and Crognale 2017). We suppose then that the coherent contour would
405 signal a uniform color field rather than just an edge-transient through the concurrent modulation of
406 ventral color areas and V1 via dorsal stream areas implicated in contour integration.

407

408 **Distributed nature of the responses.** We find responses to the stimuli distributed across multiple
409 streams and at multiple levels of the visual hierarchy, in line with an interareal network which is
410 observed to be much denser than previously thought (Markov et al. 2013) and with evidence of the
411 highly distributed nature of object processing (Konen and Kastner 2008). In area V1, the induced
412 activity of voxels remote from the contours is unlikely to be mediated by monosynaptic lateral
413 connections because intrinsic connections extend over 2 mm or less (Markov et al. 2011), and given a
414 cortical magnification factor of 6-13 mm/deg (Van Essen, Newsome, and Maunsell 1984, Daniel and
415 Whitteridge 1961), it is unlikely that lateral activity spreads much larger than a degree (Angelucci and
416 Bressloff 2006). This suggests that feedback projections from higher order areas play a role in the
417 activation of area V1. The involvement of descending pathways is highly relevant given the role of
418 feedback pathways in contextual processing (Zipser, Lamme, and Schiller 1996). Here, feedback
419 projections from areas V3A and V3B/KO could be particularly significant given that we show that these

areas code the behavioral response and that the dynamic causal model that best supports the data indicates that the effective connectivity from V3A to V1 is modulated differentially by the WCE. Recent human studies suggest that area V3A is relatively low in the cortical hierarchy (Michalareas et al. 2016) so that these findings are in line with previous evidence of activity at early hierarchical stages reflecting the content of consciousness (Leopold and Logothetis 1996). In the framework of predictive coding, that postulates that prediction errors are propagated up the cortical hierarchy and predictions down the hierarchy (Friston and Kiebel 2009), the descending prediction signal from area V3A might not be related to consciousness content but instead could be an aspect of figure-ground distinction which is thought to be represented in area V1 (Kok and de Lange 2014, Cornelissen et al. 2006, Von der Heydt and Pierson 2006) or alternatively a signal for a prior indicating the presence of a uniform color field.

Conclusion. Our results provide evidence that the visual system employs separate networks for the processing of surface colors that are generated by a field of uniform chromaticity and those due to filling-in induced by distant chromatic edges, so that the neural responses to a uniform and a filled-in color are not isomorphic. Responses in early visual areas are likely due to differential feedback processes from the dorsal and ventral streams. We, thus, conclude that surface color representation depends on a context-sensitive network of multiple distributed processes in the cortex.

Material and Methods

Observers

Sixteen observers (10 female, mean±SD age: 28±4 years) participated in the study. All observers had normal color vision (Ishihara test and Panel D15), normal or corrected to normal vision and were all right-handed. The study was approved by the local ethics committee (ID-RCB 2012-A000123-40) and all participants gave written informed consent.

Stimuli

The stimuli were created with Matlab R2010b (Mathworks, MA., U.S.A.), and displayed with the PsychToolbox extensions (Brainard 1997, Pelli 1997). Spectral and luminance calibrations of the

450 display were performed with a PR-650 SpectraScan Colorimeter (Photoresearch) and used for screen
451 gamma-correction in stimulus specification. All stimuli were displayed on a white background (580
452 cd/m2, CIE xy = 0.29, 0.30). Stimuli in the main experiment were defined by a virtual circle (8 degree
453 diameter, i.e., 4 degree eccentricity when centrally fixated) whose radius was modulated sinusoidally.
454 A subset of observers was also tested in independent sessions with a 4 degree diameter stimulus as a
455 comparison to conditions from previous psychophysical studies (Devinck et al. 2014, Gerardin et al.
456 2014). These measures served as a test for repeatability of the pattern of results. The contour pairs
457 that defined stimuli in all conditions had a combined width of 16 min, i.e., 8 min each. The classical
458 WCE was generated with a pair of continuous adjacent contours and will be referred to as the *test or*
459 *edge-dependent* condition (Figure 2b, left). The outer contour appeared purple (CIE xy = 0.32, 0.19)
460 and the inner orange (CIE xy = 0.48, 0.34). Control stimuli were defined by interleaving the interior
461 and exterior contours in a braid (Figure 2b, center) (Devinck and Knoblauch 2012). All stimuli were
462 also specified in the DKL color space (Derrington, Krauskopf, and Lennie 1984) with purple and
463 orange contours at azimuths of 320 and 45 deg, respectively. Additional information is described in the
464 *Stimuli and conditions* paragraph in the section fMRI Design and procedure: the WCE experiment.
465
466 **Psychophysical Procedures**
467 Prior to the collection of fMRI data, all observers performed the Maximum Likelihood Difference
468 Scaling (MLDS) task, (Knoblauch and Maloney 2012, 2008, Maloney and Yang 2003) in order to
469 measure the perceived magnitude of the WCE from the stimuli *in situ*, in the scanner, for each
470 observer, following the procedure introduced by Devinck and Knoblauch (2012). To confirm that
471 observers responded according to the fill-in color and not on the basis of other stimulus feature(s),
472 equal numbers of test and control stimuli were interleaved in the session. On each trial, a randomly
473 selected triad of either test or control patterns was presented with three luminance elevations of the
474 orange contour (a, b, c) chosen from a series of 10, with a < b < c. Stimulus b was always the upper
475 stimulus in the middle, and stimuli a and c were randomly positioned below on the left or right side,
476 respectively (Figure 3a). In each session, there was a random presentation of the 10!/(3! 7!) = 120
477 unique triads from the series of 10 luminances of the orange contour, equally-spaced in elevation from
478 the equiluminant plane in DKL space from 0.1 to 0.9, for both test and control stimuli triads, thus
479 yielding a total of 240 presentations. Frequency and amplitude of the contour were set to 20 cycles per

480 revolution (cpr) and 0.2, respectively, with values shown previously to generate a strong WCE
481 (Gerardin et al. 2014). On presentation of a triad, the observer was instructed to fixate each pattern
482 until he/she could choose which of the two bottom patterns (left or right) was most similar to the upper
483 pattern with respect to the color of its interior region. The observer's response initiated the next trial.
484 No feedback was provided to observers. Difference scales for test and control stimuli were estimated
485 from the session by maximum likelihood using the mlds function from the MLDS package (Knoblauch
486 and Maloney 2008) in the open source software R (RCoreTeam 2015). The scales estimated are
487 based on a signal detection model of the decision process and have the property that equal scale
488 differences are perceptually equal, i.e., they are interval scales. When parameterized so that each
489 response has unit variance, the scales can be interpreted in terms of the signal detection parameter *d'*
490 (Knoblauch and Maloney 2012). Additional details on the procedure and modeling can be found
491 elsewhere (Devinck et al. 2014, Devinck and Knoblauch 2012).
492
493 **fMRI Design and procedure**
494 Observers were presented sequences of stimuli selected from the three conditions described below.
495 To control for attentional factors, during all functional MRI experiments, observers performed a task
496 requiring them to detect a change in orientation of the fixation cross. Observers were instructed to
497 press a button when they detected a change in the fixation cross from '+' to 'x'. Performance for this
498 task was 79% ±3% (SD) correct. All stimuli were back-projected using a video-projector on a
499 translucent screen positioned at the rear of the magnet. A subject, lying on his/her back in the
500 scanner, viewed this screen via a mirror fixed on the head coil. Viewing distance was 222 cm.
501
502 *Stimuli and conditions*
503 Three conditions were used. *a) Edge-dependent stimuli*: Based on our previous studies (Gerardin et
504 al. 2014) and the psychophysical experiments performed in the scanner, stimuli were chosen to
505 generate strong WCE. Three contour frequencies (16, 18 and 20 cpr) were used, with two contour
506 amplitudes (0.16 and 0.20) and with three luminances of the orange contour (elevations of 0.7, 0.8
507 and 0.9 in DKL space) (Figure 2b left). *b) Control stimuli:* Control stimuli were identical except that the
508 contours were interlaced or braided and generated little filling-in (Figure 2b center). *c) Surface-*
509 *dependent stimuli:* These stimuli had braided contours similar to the control, but the region interior to

510 the contours was set to a uniform chromaticity and luminance that matched the interior, fill-in color of
511 the edge-dependent stimuli based on a paired-comparison experiment performed inside the scanner
512 for each subject (Figure 2b right). These stimuli were designed to generate the same appearance as
513 the uniform interior of the WCE stimulus but with the bounding contour of the control stimulus.
514 For the paired-comparisons (performed in the scanner prior to scanning), observers were
515 presented simultaneously with a test and a control stimulus (braided contour) for which the
516 appearance of the interior was controlled by adjusting the luminance elevation (in DKL color space) of
517 the interior with respect to the equiluminant plane at constant vector length, thereby continuously
518 varying the colorimetric purity of the interior region. Observers judged which interior region of the pair
519 was more orange and the match was assigned to the value at which the probability of a choice was
520 estimated to be 50%.
521
522 *Procedure*
523 Each observer was tested in one session comprising six scanning runs. Each run consisted of 12
524 blocks plus 5 fixation intervals (including one at the start, one at the end, and one between each 3-
525 block sequence) and lasting for 272 sec. Three conditions were tested: a) stimuli inducing WCE
526 (edge-dependent), b) null filling-in stimuli (control) and c) surface-dependent stimuli. Each block
527 comprised 20 stimuli of one condition and was repeated four times. Blocks were presented in a
528 randomized sequence. Each stimulus was presented for 500 ms followed by a blank interval (300 ms).
529
530 **Mapping regions of interest**
531 In a second session, for each observer, we identified: 1) retinotopic areas V1 and V2, 2) the human V4
532 (hV4, also identified by retinotopic mapping) and Lateral Occipital complex (LO) and 3) motion-related
533 areas (V3B/KO, hMT+/V5). We functionally localized early visual areas V1 and V2, dorsal retinotopic
534 areas V3, V3A and V7 and ventral retinotopic areas V3v and hV4 based on standard retinotopic
535 mapping procedures (Warnking et al. 2002, DeYoe et al. 1996, Sereno et al. 1995, Engel et al. 1994).
536 We also functionally localized LO (Kourtzi and Kanwisher 2001), V3B/KO (Dupont et al. 1997), and
537 hMT+/V5 (Tootell et al. 1995) with a block related paradigm detailed below (Figure 7).
538
539 **fMRI Data Acquisition**

540 All experiments were conducted using a 3-Tesla Philips Achieva MRI scanner at the Grenoble MRI
541 facility IRMaGE, France. In each session for each individual, a high-resolution T1-weighted
542 structural image (3D TFE sequence, acquisition matrix 240x256x180, TR/TE: 25/2.3 ms, flip angle 9°,
543 1x1x1mm resolution) and series of T2*-weighted functional images (EPI MS-FFE, acquisition matrix
544 80x80, 30 slices, TR/TE: 2000/30 ms, flip angle 80°, acquisition voxel size 3x3x2.75mm, reconstructed
545 voxel size 3x3x3mm) were collected with a 32 channel SENSE head coil.
546 In order to control for fixation stability, the position of the left eye over the course of all
547 experiments was monitored with an ASL EyeTracker 6000. No systematic deviations from the fixation
548 point were observed and no data were excluded from the analysis.
549
550 **fMRI Data Analysis**
551 The fMRI data were analyzed using Brain Voyager QX (Brain Innovations, Maastricht, The
552 Netherlands). Preprocessing of the functional data consisted of slice-scan time correction, head
553 movement correction, temporal high-pass filtering (2 cycles) and linear trend removal. Individual
554 functional images were aligned to each corresponding anatomical image that was used for 3D cortex
555 reconstruction, inflation and flattening. The volume time-course datasets were convolved with a
556 canonical hemodynamic response function. No spatial smoothing was applied except for the group
557 whole brain analysis (Gaussian filter; full-width at half maximum: 6 mm kernel) after normalization of
558 all data to a common referential (Talairach space). Multi-Vovel Pattern Analyses (MVPA) were
559 performed on each individual with Matlab R2010b (www.MathWorks.com) and SVM^{light} (Joachims
560 1999). Dynamic Causal Modelling (DCM) analyses were performed using Matlab (R2014a-
561 with SPM12 (6906) with supplementary analyses using the open source software R (R Core Team,
562 2017).
563
564 *Mapping Regions of Interest*
565 For retinotopic areas we computed correlation analyses with a sinusoidal function with 16 lags to
566 obtain power and phase maps for both the eccentricity and the polar mapping. Phase maps were
567 thresholded at a correlation of 0.2 and projected on the cortical flat maps. The borders between visual
568 areas were identified as phase reversals on the polar phase maps, with simultaneous visualization of
569 the eccentricity map to ensure that the borders ran perpendicularly to the eccentricity gradient. We

570 identified V1 and V2, dorsal areas up to V7 and ventral areas up to hV4. In addition, for area V1, a set
571 of voxels was selected that was retinotopically interior to those significantly activated by the contours
572 of the control stimulus (4-degree eccentricity, blue shading in Figure 7) for use in the subsequent
573 MVPA analysis. This selection was based on the data from the retinotopic mapping experiments, i.e.,
574 eccentricity maps defined using expanding concentric rings. This allows excluding for classification
575 patterns on the basis of voxels that respond in each condition to the contour *per se*.
576
577 Using the general linear model (GLM) including fixation periods and movement correction parameters
578 as covariates of no interest, we identified LOC, hMT+/V5 and V3B/KO. LOC was defined as the set of
579 contiguous voxels in the ventral occipito-temporal cortex that showed significantly stronger activation
580 ($t(165)>4.0$, $p<0.001$ uncorrected) for intact compared to scrambled images of objects (Kourtzi and
581 Kanwisher 2001). hMT+/V5 (Tootell et al. 1995) was defined as the set of contiguous voxels in the
582 lateral occipito-temporal cortex that showed significantly stronger activation ($t(165)>4.0$, $p<0.001$
583 uncorrected) for moving than for static random dots. V3B/KO was defined as the set of contiguous
584 voxels anterior to V3A that showed significantly stronger activation ($t(165)>4.0$, $p<0.001$ uncorrected)
585 for random-dot displays that defined relative rather than transparent motion (Dupont et al. 1997).
586
587 *Multi-voxel pattern analysis*
588 Multi-voxel Pattern Analysis (Haynes and Rees 2005, Kamitani and Tong 2005), using linear Support
589 Vector Machine (SVM) classifiers followed by cross-validation procedures, was used with Matlab
590 R2010b (www.MathWorks.com) (Gerardin, Kourtzi, and Mamassian 2010) and SVM^{light} (Joachims
591 1999). For each Region of Interest (ROI: retinotopic areas, LO, V3B/KO and hMT+/V5), voxels were
592 sorted according to their response (t-statistic maps based on the GLM) to all stimulus conditions
593 compared to fixation baseline across all experimental runs. The number of voxels was selected across
594 individual ROIs and observers by restricting the pattern size to those voxels that showed a significant
595 ($p<0.05$ uncorrected) t value. One hundred voxels from both hemispheres were included for each ROI
596 and subject. For area V1, voxels were chosen to be at retinotopic eccentricities inferior to those
597 activated directly by the control stimulus contour at 4 degrees (blue region of V1 in Figure 7). For other
598 visual areas, it was not possible to exclude such voxels for all observers and maintain 100 voxels per
599 ROI. Each voxel time course was normalized (z-score) separately for each experimental run in order

600 to minimize baseline differences. For each subject and each condition, all time series data points of
601 the corresponding experimental block were averaged in order to generate the data vectors for the
602 multivariate analysis. Data vectors were selected according to the comparison of interest and split into
603 a training sample comprising the data of five runs and a test sample comprising the remaining run. A
604 six-fold cross-validation was performed leaving one run out (test sample). For each subject, accuracy
605 rates were averaged (number of correctly assigned test patterns/total number of assignments) across
606 the cross-validation runs. Statistical significance across conditions was evaluated using linear mixed-
607 effects models with observer treated as a random effect (Pinheiro and Bates 2000). A recent study
608 questioned the use of parametric significance tests with MVPA based on simulations that revealed
609 skewness of the null-distribution (Jamalabadi et al. 2016). Diagnostic plots of the residuals from the
610 mixed-effect model fits (residuals vs fitted values, and quantile-quantile plots, not shown), however,
611 revealed no systematic deviations from model distribution or variance assumptions that would warrant
612 discounting the model or preferring transformed values of the response variable.
613
614
615 *Control analyses for the MVPA*
616 Control analyses were obtained by shuffling to ensure that the classification accuracies observed were
617 not due to random statistical regularities in the data. The same classifiers were run with randomly
618 assigned category labels to the activation pattern. Accuracies were not significantly different from
619 chance, supporting that the classification results could not be attributed to random patterns in the data.
620
621 *Dynamic Causal Modeling for BOLD responses*
622 Using Dynamic Causal Modeling (DCM), we explored changes in the effective connectivity, i.e. the
623 influence exerted by one region on the others, and how information is propagated through these
624 regions (see (Friston 2011) for details about the operational distinction between functional and
625 effective connectivity) in response to our protocol. DCM considers the brain as a deterministic system
626 whose response in a region or part of a cortical network, is determined by inputs to that region. We
627 defined causal models of connectivity between selected ROIs to make inferences about underlying
628 mechanisms expressed in our BOLD data. These models included 1) intrinsic (or endogenous)
629 connections that quantify the effective fixed connectivity between the model nodes, i.e. the changes in

activity in a target region when activity in the source region changes (matrix A in DCM), 2) stimulus-related inputs that define how the model responds to task-related inputs (matrix C in DCM), and 3) possible input modulations that define how the effective connectivity is influenced by experimental factors (matrix B in DCM). Following model estimations, DCM provides a Bayesian method (Bayesian Model Selection, BMS) for selecting the best model of coupling that explains connectivity changes underlying task-related brain responses (Friston, Harrison, and Penny 2003). Note that effective connectivity between regions does not imply underlying direct anatomical connections (Friston 2011).

Model structure: Following BMS, each model is attributed a probability according to its power to describe the data. These probabilities sum to one, so the number of models in the model space must be limited to prevent excessive dilution of the maximum probability. One way to achieve this is to limit the number of areas considered. In our case, three regions were considered in each model definition because it is the lowest number necessary to translate our hypothesis concerning the connectivity modulations between dorsal and ventral streams. For example, region V1 (as receiving visual input), region V3A (that best classified edge-dependent stimuli) and region LO (that best classified surface-dependent stimuli). As early visual areas are strongly interconnected, we considered all possible connections between and within areas in our endogenous matrix. Our control stimuli entered all models as a driving input to V1.

Connectivity Modulation: We designed a model space in terms of which a subset of connections was modulated by the edge-dependent or the surface-dependent stimuli. We reasoned that both types of stimuli have a differential effect on endogenous connections of the network for each subject. We did not consider bidirectional modulations because we were only interested in the strongest direction. V1 was always connected to the two other areas in all models, but we included the hypothesis that there was no differential modulation between them. Because of the importance of V1 intrinsic horizontal connections for contour integration (Stettler et al. 2002), for each model we included a self-modulation of V1. This resulted in the model space described in Figures 6a and S2a with 12 possible modulations.

Model comparison: All twelve models were applied successively with the functional datasets from each subject and each condition (edge-induced or surface-dependent). They entered a Bayesian

model selection procedure that identified which of the competing models best predicts each dataset. For each model, the model evidence, i.e. the probability of observing the measured data given a specific model, was computed based on the free energy approximation. Model evidence was used by the Bayesian model selection procedure to rank the models. The protected exceedance probability defined the relative superiority that a model was more likely that any other model considered, given the group data (Rigoux et al. 2014). For group-level Bayesian model selection we then considered a Random-effects (RFX) analysis to account for between-subject variability (Stephan et al. 2009).

Acknowledgements: This work was supported by a grant from the Agence Nationale de la Recherche to FD (ANR-11-JSH-20021) and by LABEX CORTEX (ANR-11-LABX-0042) to KK and HK and ANR-11-BSV4-501, CORE-NETS (H.K.), ANR-14-CE13-0033, ARCHI-CORE (H.K.), ANR-15-CE32-0016, CORNET (H.K.). The Grenoble MRI facility IRMaGe was partly funded by the French program 'Investissement d'Avenir' run by the Agence Nationale pour la Recherche (ANR-11-INBS-0006). The authors thank Elisabeth Baumgartner, Karl Gegenfurtner and Stewart Shipp for comments and criticisms for a previous version of this manuscript. They also thank Mathieu Ruiz for help with data analysis and the technical staff at the Grenoble MRI facility IRMaGe.

References

Angelucci, A., and P. C. Bressloff. 2006. "Contribution of feedforward, lateral and feedback connections to the classical receptive field center and extra-classical receptive field surround of primate V1 neurons." *Prog Brain Res* 154:93-120. doi: 10.1016/S0079-6123(06)54005-1.

Anstis, S. 2010. "Visual filling-in." *Curr Biol* 20 (16):R664-6. doi: 10.1016/j.cub.2010.06.029.

Bartels, A., and S. Zeki. 2000. "The architecture of the colour centre in the human visual brain: new results and a review." *Eur J Neurosci* 12 (1):172-93.

Bellot, E., V. Coizet, J. Warnking, K. Knoblauch, E. Moro, and M. Dojat. 2016. "Effects of aging on low luminance contrast processing in humans." *Neuroimage* 139:415-426. doi: 10.1016/j.neuroimage.2016.06.051.

Bouvier, S. E., K. S. Cardinal, and S. A. Engel. 2008. "Activity in visual area V4 correlates with surface perception." *J Vis* 8 (7):28 1-9. doi: 10.1167/8.7.28.

Brainard, D. H. 1997. "The Psychophysics Toolbox." *Spat Vis* 10 (4):433-6.

Brouwer, G. J., and D. J. Heeger. 2009. "Decoding and reconstructing color from responses in human visual cortex." *J Neurosci* 29 (44):13992-4003. doi: 10.1523/JNEUROSCI.3577-09.2009.

Brown, H., and K. J. Friston. 2012. "Free-energy and illusions: the Cornsweet effect." *Front Psychol* 3:43. doi: 10.3389/fpsyg.2012.00043.

Caplovitz, G. P., and P. U. Tse. 2007. "V3A processes contour curvature as a trackable feature for the perception of rotational motion." *Cereb Cortex* 17 (5):1179-89. doi: 10.1093/cercor/bhl029.

Castaldi, E., F. Frijia, D. Montanaro, M. Tosetti, and M. C. Morrone. 2013. "BOLD human responses to chromatic spatial features." *Eur J Neurosci* 38 (2):2290-9. doi: 10.1111/ejn.12223.

Chevreul, M.E. . 1839. *De la loi du contraste simultané des couleurs et de l'assortiment des objets coloré.* Paris: Hachette Livre BNF (éd. 2012).

Coia, A. J., and M. A. Crognale. 2017. "Contour adaptation reduces the spreading of edge induced colors." *Vision Res*. doi: 10.1016/j.visres.2017.01.009.

Coia, A. J., C. Jones, C. S. Duncan, and M. A. Crognale. 2014. "Physiological correlates of watercolor effect." *J Opt Soc Am A Opt Image Sci Vis* 31 (4):A15-22. doi: 10.1364/JOSAA.31.000A15.

Cornelissen, F. W., A. R. Wade, T. Vladusich, R. F. Dougherty, and B. A. Wandell. 2006. "No functional magnetic resonance imaging evidence for brightness and color filling-in in early human visual cortex." *J Neurosci* 26 (14):3634-41. doi: 10.1523/JNEUROSCI.4382-05.2006.

Daniel, P. M., and D. Whitteridge. 1961. "The representation of the visual field on the cerebral cortex in monkeys." *J Physiol* 159:203-21.

De Weerd, P., R. Gattass, R. Desimone, and L. G. Ungerleider. 1995. "Responses of cells in monkey visual cortex during perceptual filling-in of an artificial scotoma." *Nature* 377 (6551):731-4. doi: 10.1038/377731a0.

Derrington, A. M., J. Krauskopf, and P. Lennie. 1984. "Chromatic mechanisms in lateral geniculate nucleus of macaque." *J Physiol* 357:241-65.

Devinck, F., P. Gerardin, M. Dojat, and K. Knoblauch. 2014. "Spatial selectivity of the watercolor effect." *J Opt Soc Am A Opt Image Sci Vis* 31 (4):A1-6. doi: 10.1364/JOSAA.31.0000A1.

Devinck, F., and K. Knoblauch. 2012. "A common signal detection model accounts for both perception and discrimination of the watercolor effect." *J Vis* 12 (3). doi: 10.1167/12.3.19.

DeYoe, E. A., G. J. Carman, P. Bandettini, S. Glickman, J. Wieser, R. Cox, D. Miller, and J. Neitz. 1996. "Mapping striate and extrastriate visual areas in human cerebral cortex." *Proc Natl Acad Sci U S A* 93 (6):2382-6.

Dupont, P., B. De Bruyn, R. Vandenberghe, A. M. Rosier, J. Michiels, G. Marchal, L. Mortelmans, and G. A. Orban. 1997. "The kinetic occipital region in human visual cortex." *Cereb Cortex* 7 (3):283-92.

Engel, S. A., D. E. Rumelhart, B. A. Wandell, A. T. Lee, G. H. Glover, E. J. Chichilnisky, and M. N. Shadlen. 1994. "fMRI of human visual cortex." *Nature* 369 (6481):525. doi: 10.1038/369525a0.

Friedman, H. S., H. Zhou, and R. von der Heydt. 2003. "The coding of uniform colour figures in monkey visual cortex." *J Physiol* 548 (Pt 2):593-613. doi: 10.1113/jphysiol.2002.033555.

Friston, K. J. 2011. "Functional and effective connectivity: a review." *Brain Connect* 1 (1):13-36. doi: 10.1089/brain.2011.0008.

Friston, K. J., L. Harrison, and W. Penny. 2003. "Dynamic causal modelling." *Neuroimage* 19 (4):1273-302.

Friston, K., and S. Kiebel. 2009. "Predictive coding under the free-energy principle." *Philos Trans R Soc Lond B Biol Sci* 364 (1521):1211-21. doi: 10.1098/rstb.2008.0300.

Gerardin, P., F. Devinck, M. Dojat, and K. Knoblauch. 2014. "Contributions of contour frequency, amplitude, and luminance to the watercolor effect estimated by conjoint measurement." *J Vis* 14 (4). doi: 10.1167/14.4.9.

Gerardin, P., Z. Kourtzi, and P. Mamassian. 2010. "Prior knowledge of illumination for 3D perception in the human brain." *Proc Natl Acad Sci U S A* 107 (37):16309-14. doi: 10.1073/pnas.1006285107.

Hadjikhani, N., A. K. Liu, A. M. Dale, P. Cavanagh, and R. B. Tootell. 1998. "Retinotopy and color sensitivity in human visual cortical area V8." *Nat Neurosci* 1 (3):235-41. doi: 10.1038/681.

Haynes, J. D., and G. Rees. 2005. "Predicting the orientation of invisible stimuli from activity in human primary visual cortex." *Nat Neurosci* 8 (5):686-91. doi: 10.1038/nn1445.

Holm, S. 1979. "A simple sequentially rejective multiple test procedure." *Scandinavian Journal of Statistics* 6:65-70.

Jamalabadi, H., S. Alizadeh, M. Schonauer, C. Leibold, and S. Gais. 2016. "Classification based hypothesis testing in neuroscience: Below-chance level classification rates and overlooked statistical properties of linear parametric classifiers." *Hum Brain Mapp* 37 (5):1842-55. doi: 10.1002/hbm.23140.

Joachims, T. 1999. *Making large-scale SVM learning practical. Advances in Kernel Methods – Support Vector Learning.* MIT Press.: B. Schölkopf, C. Burges and A. Smola.

Johnson, E. N., M. J. Hawken, and R. Shapley. 2001. "The spatial transformation of color in the primary visual cortex of the macaque monkey." *Nat Neurosci* 4 (4):409-16. doi: 10.1038/86061.

Kamitani, Y., and F. Tong. 2005. "Decoding the visual and subjective contents of the human brain." *Nat Neurosci* 8 (5):679-85. doi: 10.1038/nn1444.

Knoblauch, K., and L.T. Maloney. 2008. "MLDS: Maximum likelihood difference scaling in R." *Journal of Statistical Software* 25 (2):1-26.

Knoblauch, K., and L.T. Maloney. 2012. "Modeling Psychophysical Data in R." *New York: Springer*.

Kok, P., and F. P. de Lange. 2014. "Shape perception simultaneously up- and downregulates neural activity in the primary visual cortex." *Curr Biol* 24 (13):1531-5. doi: 10.1016/j.cub.2014.05.042.

Komatsu, H. 2006. "The neural mechanisms of perceptual filling-in." *Nat Rev Neurosci* 7 (3):220-31. doi: 10.1038/nrn1869.

Konen, C. S., and S. Kastner. 2008. "Two hierarchically organized neural systems for object information in human visual cortex." *Nat Neurosci* 11 (2):224-31. doi: 10.1038/nn2036.

Kourtzi, Z., and N. Kanwisher. 2001. "Representation of perceived object shape by the human lateral occipital complex." *Science* 293 (5534):1506-9. doi: 10.1126/science.1061133.

Kravitz, D. J., K. S. Saleem, C. I. Baker, L. G. Ungerleider, and M. Mishkin. 2013. "The ventral visual pathway: an expanded neural framework for the processing of object quality." *Trends Cogn Sci* 17 (1):26-49. doi: 10.1016/j.tics.2012.10.011.

Lee, T. S., and M. Nguyen. 2001. "Dynamics of subjective contour formation in the early visual cortex." *Proc Natl Acad Sci U S A* 98 (4):1907-11. doi: 10.1073/pnas.031579998.

Leopold, D. A., and N. K. Logothetis. 1996. "Activity changes in early visual cortex reflect monkeys' percepts during binocular rivalry." *Nature* 379 (6565):549-53. doi: 10.1038/379549a0.

Maloney, L. T., and J. N. Yang. 2003. "Maximum likelihood difference scaling." *J Vis* 3 (8):573-85. doi: 10:1167/3.8.5.

Markov, N. T., M. Ercsey-Ravasz, D. C. Van Essen, K. Knoblauch, Z. Toroczkai, and H. Kennedy. 2013. "Cortical high-density counterstream architectures." *Science* 342 (6158):1238406. doi: 10.1126/science.1238406.

Markov, N. T., P. Misery, A. Falchier, C. Lamy, J. Vezoli, R. Quilodran, M. A. Gariel, P. Giroud, M. Ercsey-Ravasz, L. J. Pilaz, C. Huissoud, P. Barone, C. Dehay, Z. Toroczkai, D. C. Van Essen, H. Kennedy, and K. Knoblauch. 2011. "Weight consistency specifies regularities of macaque cortical networks." *Cerebral Cortex* 21 (6):1254-72. doi: 10.1093/cercor/bhq201.

Mendola, J. D., I. P. Conner, S. Sharma, A. Bahekar, and S. Lemieux. 2006. "fMRI Measures of perceptual filling-in in the human visual cortex." *J Cogn Neurosci* 18 (3):363-75. doi: 10.1162/089892906775990624.

Michalareas, G., J. Vezoli, S. van Pelt, J-M. Schoffelen, H. Kennedy, and P. Fries. 2016. "Alpha-beta and gamma rhythms subserve feedback and feedforward influences among human visual areas." *Neuron* 89 (2):384-397.

Nieuwenhuis, S., B. U. Forstmann, and E. J. Wagenmakers. 2011. "Erroneous analyses of interactions in neuroscience: a problem of significance." *Nat Neurosci* 14 (9):1105-7. doi: 10.1038/nn.2886.

Parkes, L. M., J. B. Marsman, D. C. Oxley, J. Y. Goulermas, and S. M. Wuerger. 2009. "Multivoxel fMRI analysis of color tuning in human primary visual cortex." *J Vis* 9 (1):1 1-13. doi: 10.1167/9.1.1.

Pelli, D. G. 1997. "The VideoToolbox software for visual psychophysics: transforming numbers into movies." *Spat Vis* 10 (4):437-42.

Peng, X., and D. C. Van Essen. 2005. "Peaked encoding of relative luminance in macaque areas V1 and V2." *J Neurophysiol* 93 (3):1620-32. doi: 10.1152/jn.00793.2004.

Pinheiro, J.C., and D.M. Bates. 2000. *Mixed-Effects Models in S and S-PLUS*. New York: Springer.

Pinna, B., G. Brelstaff, and L. Spillmann. 2001. "Surface color from boundaries: a new 'watercolor' illusion." *Vision Res* 41 (20):2669-76.

Pinna, B., and S. Grossberg. 2005. "The watercolor illusion and neon color spreading: a unified analysis of new cases and neural mechanisms." *J Opt Soc Am A Opt Image Sci Vis* 22 (10):2207-21.

Press, W. A., A. A. Brewer, R. F. Dougherty, A. R. Wade, and B. A. Wandell. 2001. "Visual areas and spatial summation in human visual cortex." *Vision Res* 41 (10-11):1321-32.

Ratliff, F., and L. Sirovich. 1978. "Equivalence classes of visual stimuli." *Vision Res* 18 (7):845-51.

RCoreTeam. 2015. "R: A Language and Environment for Statistical Computing, R Foundation for Statistical Computing, Vienna, Austria." *ISBN 3-900051-07-0*.

Rigoux, L., K. E. Stephan, K. J. Friston, and J. Daunizeau. 2014. "Bayesian model selection for group studies - revisited." *Neuroimage* 84:971-85. doi: 10.1016/j.neuroimage.2013.08.065.

Roe, A. W., and D. Y. Ts'o. 1999. "Specificity of color connectivity between primate V1 and V2." *J Neurophysiol* 82 (5):2719-30.

Sakai, K., E. Watanabe, Y. Onodera, I. Uchida, H. Kato, E. Yamamoto, H. Koizumi, and Y. Miyashita. 1995. "Functional mapping of the human colour centre with echo-planar magnetic resonance imaging." *Proc Biol Sci* 261 (1360):89-98. doi: 10.1098/rspb.1995.0121.

Sapountzis, P., D. Schluppeck, R. Bowtell, and J. W. Peirce. 2010. "A comparison of fMRI adaptation and multivariate pattern classification analysis in visual cortex." *Neuroimage* 49 (2):1632-40. doi: 10.1016/j.neuroimage.2009.09.066.

Sasaki, Y., and T. Watanabe. 2004. "The primary visual cortex fills in color." *Proc Natl Acad Sci U S A* 101 (52):18251-6. doi: 10.1073/pnas.0406293102.

Schluppeck, D., and S. A. Engel. 2002. "Color opponent neurons in V1: a review and model reconciling results from imaging and single-unit recording." *J Vis* 2 (6):480-92. doi: 10.1167/2.6.5.

Sereno, M. I., A. M. Dale, J. B. Reppas, K. K. Kwong, J. W. Belliveau, T. J. Brady, B. R. Rosen, and R. B. Tootell. 1995. "Borders of multiple visual areas in humans revealed by functional magnetic resonance imaging." *Science* 268 (5212):889-93.

Stephan, K. E., W. D. Penny, J. Daunizeau, R. J. Moran, and K. J. Friston. 2009. "Bayesian model selection for group studies." *Neuroimage* 46 (4):1004-17. doi: 10.1016/j.neuroimage.2009.03.025.

Stephan, K. E., W. D. Penny, R. J. Moran, H. E. den Ouden, J. Daunizeau, and K. J. Friston. 2010. "Ten simple rules for dynamic causal modeling." *Neuroimage* 49 (4):3099-109. doi: 10.1016/j.neuroimage.2009.11.015.

Stettler, D. D., A. Das, J. Bennett, and C. D. Gilbert. 2002. "Lateral connectivity and contextual interactions in macaque primary visual cortex." *Neuron* 36 (4):739-50.

Takemura, H., A. Rokem, J. Winawer, J. D. Yeatman, B. A. Wandell, and F. Pestilli. 2015. "A Major Human White Matter Pathway Between Dorsal and Ventral Visual Cortex." *Cereb Cortex*. doi: 10.1093/cercor/bhv064.

Tootell, R. B., K. Nelissen, W. Vanduffel, and G. A. Orban. 2004. "Search for color 'center(s)' in macaque visual cortex." *Cereb Cortex* 14 (4):353-63.

Tootell, R. B., J. B. Reppas, K. K. Kwong, R. Malach, R. T. Born, T. J. Brady, B. R. Rosen, and J. W. Belliveau. 1995. "Functional analysis of human MT and related visual cortical areas using magnetic resonance imaging." *J Neurosci* 15 (4):3215-30.

Van Essen, D. C., W. T. Newsome, and J. H. Maunsell. 1984. "The visual field representation in striate cortex of the macaque monkey: asymmetries, anisotropies, and individual variability." *Vision Res* 24 (5):429-48.

Varin, D. 1971. "Fenomeni di contrasto e diffusione cromatica nell'organizzazione spaziale del campo percettivo." *Rivista di Psicologia* 65:101-128.

Von der Heydt, R., and R. Pierson. 2006. "Dissociation of color and figure-ground effects in the watercolor illusion." *Spat Vis* 19 (2-4):323-40.

Warnking, J., M. Dojat, A. Guerin-Dugue, C. Delon-Martin, S. Olympieff, N. Richard, A. Chehikian, and C. Segebarth. 2002. "fMRI retinotopic mapping--step by step." *Neuroimage* 17 (4):1665-83.

Yang, J. N., N. M. Szeverenyi, and D. Ts'o. 2008. "Neural resources associated with perceptual judgment across sensory modalities." *Cereb Cortex* 18 (1):38-45. doi: 10.1093/cercor/bhm029.

Zipser, K., V. A. Lamme, and P. H. Schiller. 1996. "Contextual modulation in primary visual cortex." *J Neurosci* 16 (22):7376-89.

Zweig, S., G. Zurawel, R. Shapley, and H. Slovin. 2015. "Representation of Color Surfaces in V1: Edge Enhancement and Unfilled Holes." *J Neurosci* 35 (35):12103-15.

867 **Figures**

868

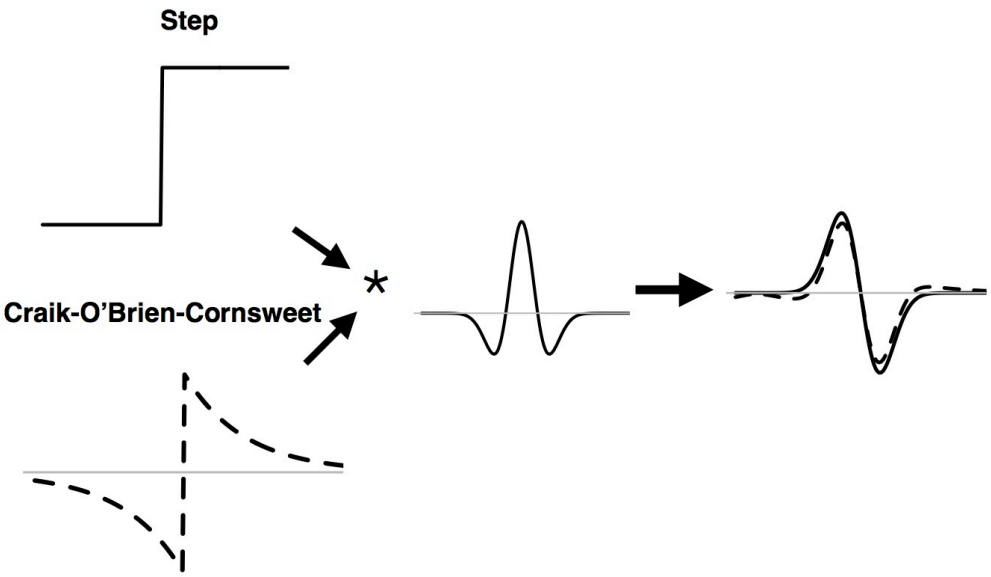

869

870 **Figure 1: Equivalence of responses for step and gradient intensity profiles under convolution**

871 **with a center-surround weighting function.**

872 Both a step change in intensity (solid curve, upper left) and the exponential ramp transient for a Craik-

873 O'Brien-Cornsweet effect (dashed curve, lower left) when convolved (indicated by "*") with a center-

874 surround weighting function (center, the negative second derivative of a Gaussian) yield nearly

875 identical response profiles (right, solid and dashed curves, respectively).

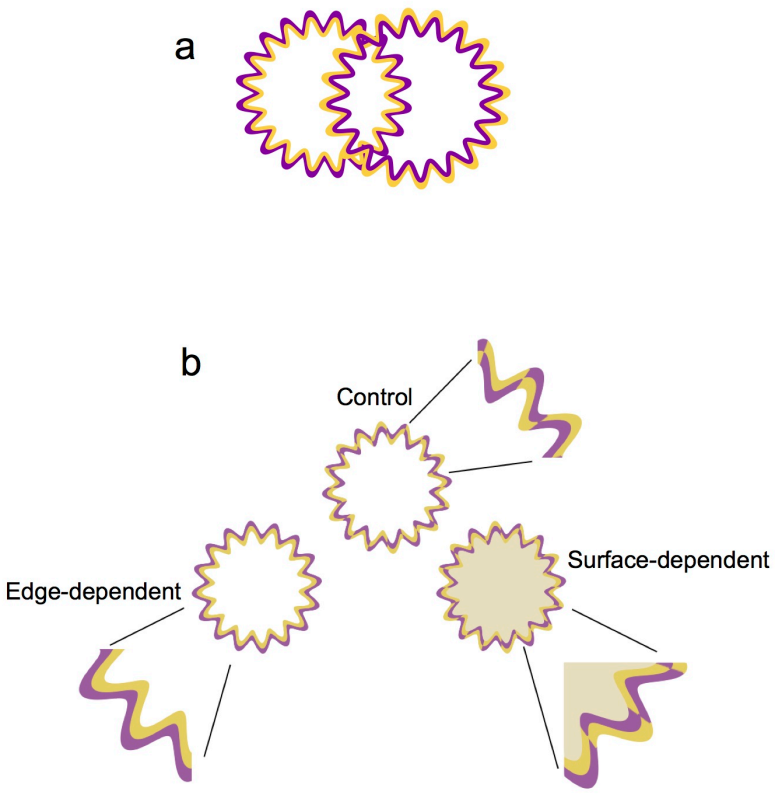

Figure 2: Watercolor effect demonstration and fMRI stimuli used in the main experiment. a. Stimulus demonstrating the WCE. Two intersecting circular chromatic contours, each with its radius frequency modulated, thereby defining three regions. In the left region, the interior region takes on the hue of the bright orange interior contours showing the WCE while in the right, the dark purple contours generate no filling-in. The region of intersection that is enclosed by both types of contours is described by some observers as showing a weaker filling-in color. b. Examples of the three classes of stimuli used in the fMRI experiment. Beside each stimulus an enlarged detail of the contour is drawn to illustrate its structure Left: Edge-dependent stimulus inducing the perception of the WCE, as defined from (Gerardin et al. 2014); Center: The control stimulus is composed of braided contours and demonstrates a decrease in strength of WCE filling-in; Right: The surface-dependent stimulus was used to match the effect of the WCE filling-in, in which the interior chromaticity was defined from each subject's matches (from a preliminary paired comparison experiment inside the scanner). These examples are schematic in terms of the width and color of the contours and interior region, which are enhanced here for visibility of the stimulus structure used.

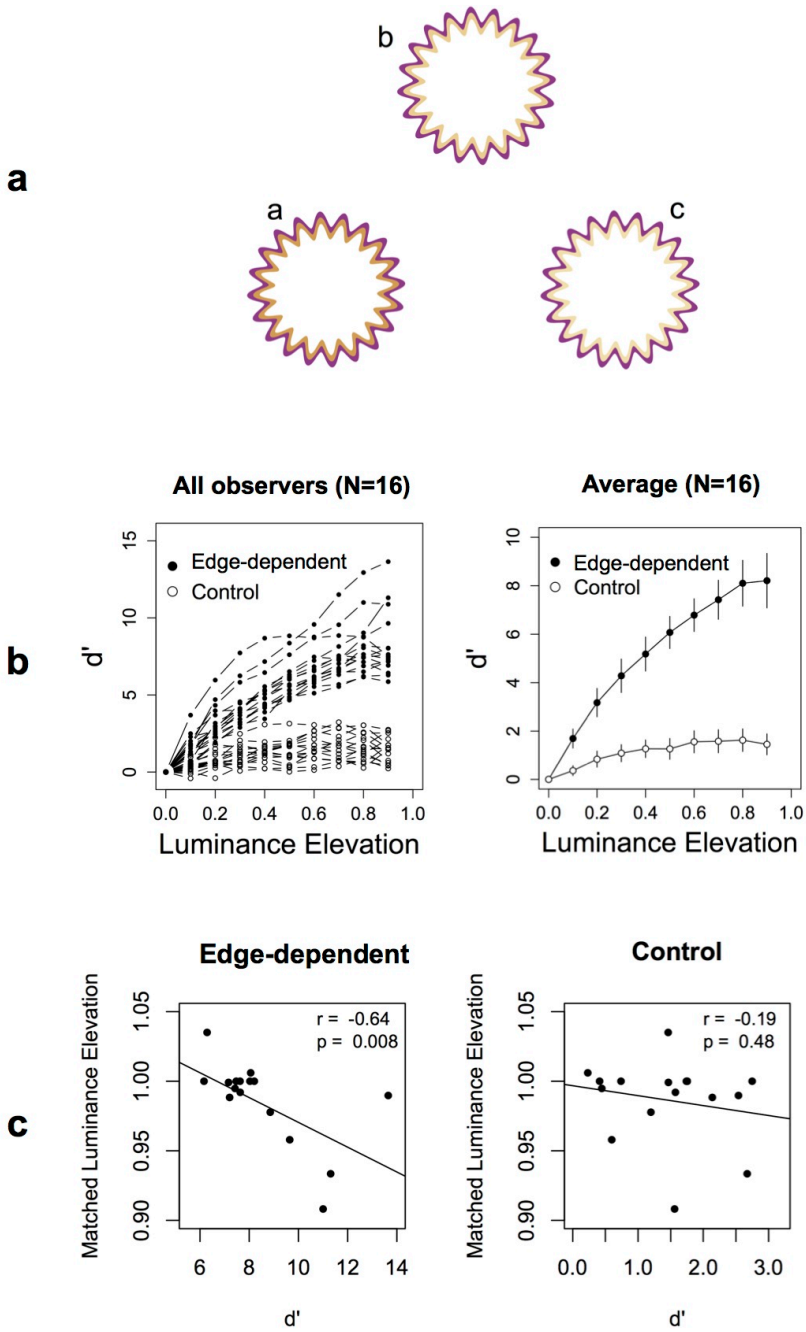

Figure 3: Psychophysics: stimulus configuration and estimated perceptual scales. (a) Example of the triad configuration used in the MLDS task performed in the session before scanning. A triad consisted of either edge-dependent (WCE) or braided control stimuli with three unique ordered luminance elevations (a, b, c, selected randomly from 10 elevations in total) of the interior orange contour. Stimulus b was always the upper stimulus in the middle, and stimuli a and c were randomly positioned on the left or right. The observer had to fixate each pattern until he/she could choose which of the two bottom patterns (left or right) was most similar to the upper pattern with respect to the color of its interior region. (b) Left all response scales for the sixteen observers as a

function of luminance elevation for edge-dependent stimuli (black) and control stimuli (white). The signal detection model used to fit the observer's data permits the ordinate values to be expressed in terms of the signal detection measure d'. Right average response scales for the sixteen observers as a function of luminance elevation for edge-dependent and control stimuli with 95% confidence intervals. (c) Correlations of MLDS results with paired-comparison matches. Results for each observer of the luminance elevation that best matched the edge-dependent stimuli (WCE) against the peak MLDS response for edge-dependent (left) and for control stimuli (right).

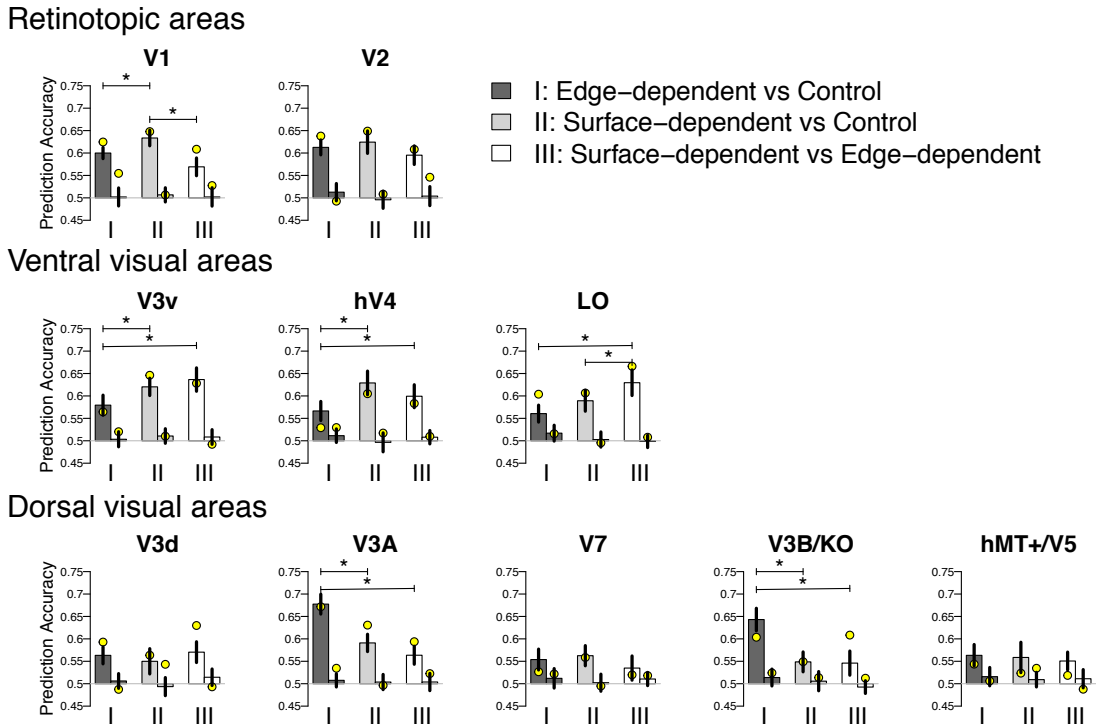

Figure 4: Multi-Voxel Pattern Analysis (MVPA) from fMRI data.

Classification accuracies across the 10 regions of interest for the three classifiers: (I) Edge-dependent vs. control (dark grey); (II) Surface-dependent vs. control (grey); (III) Surface-dependent vs. edge-dependent (white). Mean classification accuracy is based on 100 voxels per area in both hemispheres. Each bar plot shows results for 3 pairs, unshuffled (left) and shuffled (right), of classifiers. Error bars indicate 95% confidence intervals. Significant differences ($p < 0.05$) controlled for multiple comparisons (Tukey test) indicated by horizontal bars and star. The yellow points indicate average results of a repeated experiment on three of the observers using a 4 deg stimulus.

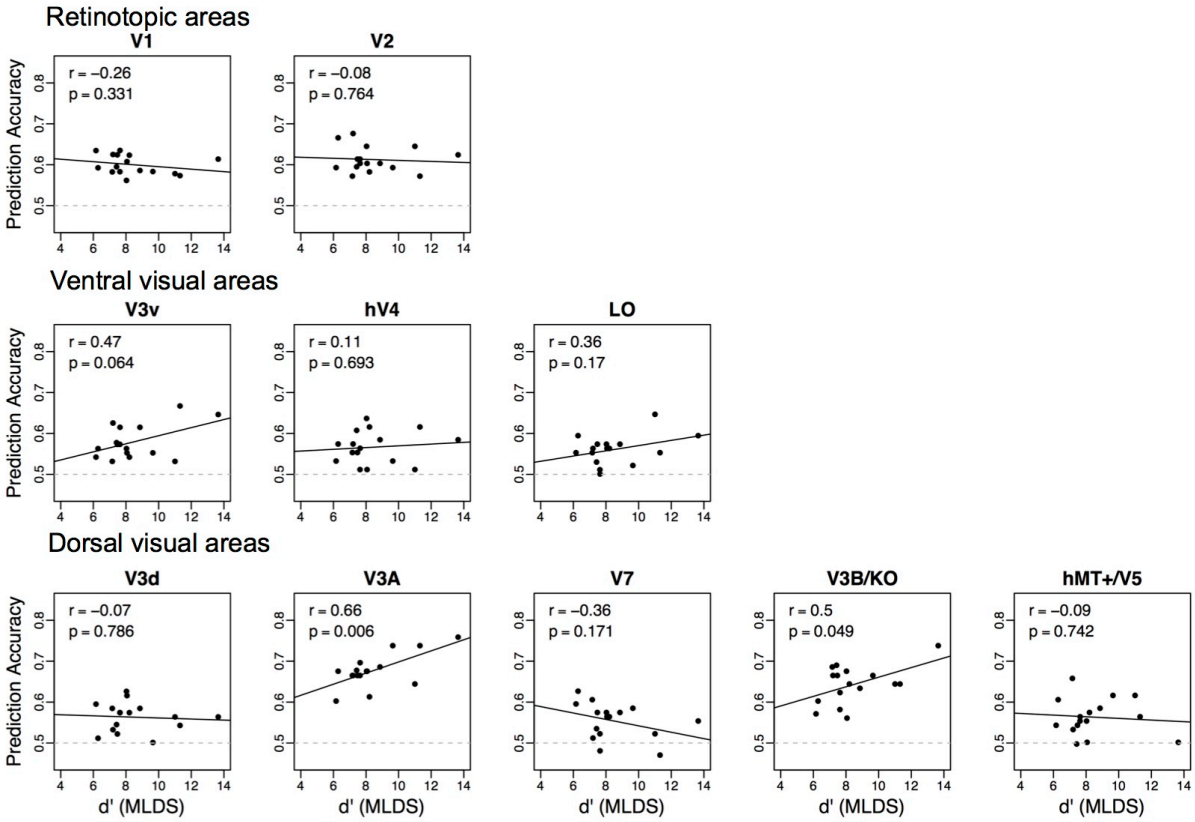

Figure 5: Correlating pattern classification and appearance.

Scatter plots of classification accuracies and peak MLDS scale values for all subjects (N=16) for the rule edge-dependent (WCE) vs. control stimulus for all ROIs with the best-fitting linear regression (solid line). Pearson product-moment correlations and p-values for the hypothesis that the correlation is 0 are indicated within each graph.

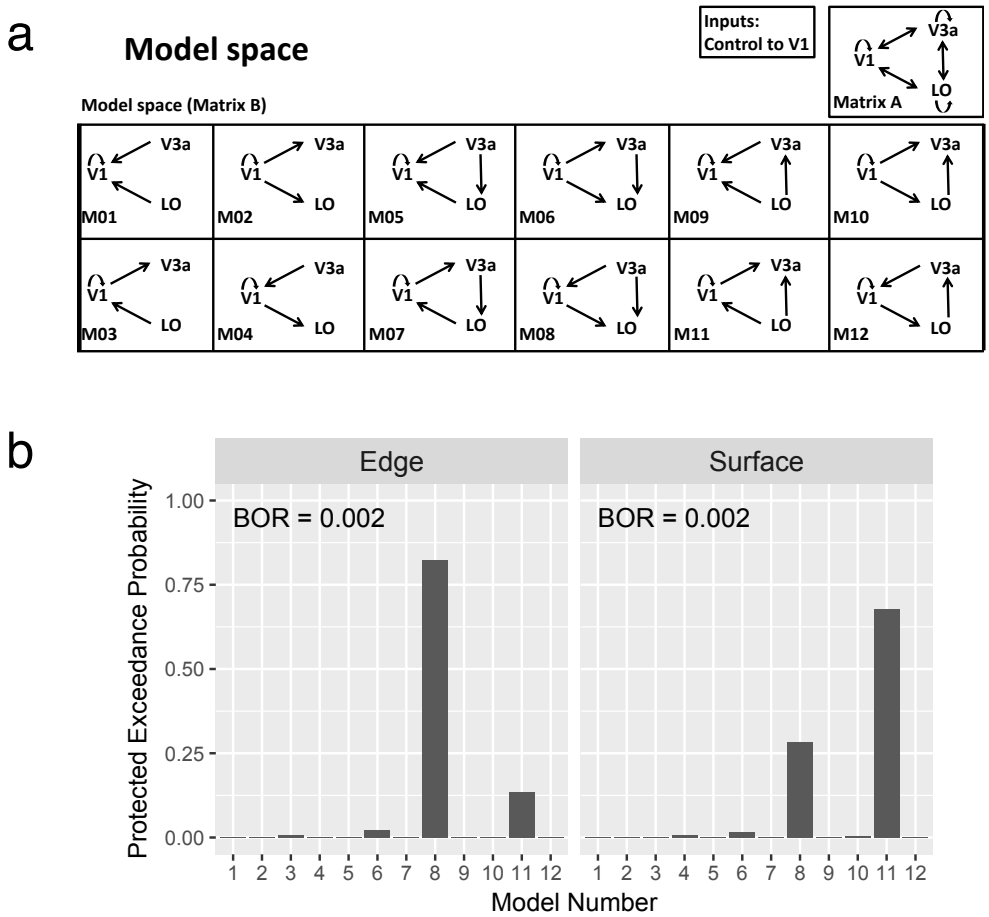

Figure 6. DCM Model space and protected exceedance probabilities for areas V1-V3A-LO. a) Twelve models (M0-M12) of the modulations of effective connectivities between areas V1, V3A and LO were evaluated in the DCM analysis. The intrinsic connectivity (Matrix A) was taken to be complete within and between areas. Activations in response to the Control condition (braided stimuli, no perceived color) were used as input in V1, while activations in response to the Edge dependent or Surface dependent conditions could modulate effective connectivity (Matrix B) according to each model. Each model included self-modulation in V1 and unilateral modulations between V1 and area V3A and between V1 and area LO, yielding 4 possible combinations. Additionally there could either be no modulation between area V3A and area LO (M01 to M04), unilateral modulation from area V3A to area LO (M05 to M08) or unilateral modulation from area LO to area V3A (M09 to M12). b) Protected exceedance probabilities (PEP) for each of the 12 models of modulation of the effective connectivities between the triple of areas indicated in (a) for the edge dependent (left) and surface dependent (right) stimuli. The Bayesian Omnibus Risk (BOR) is indicated in the upper left corner of each plot.

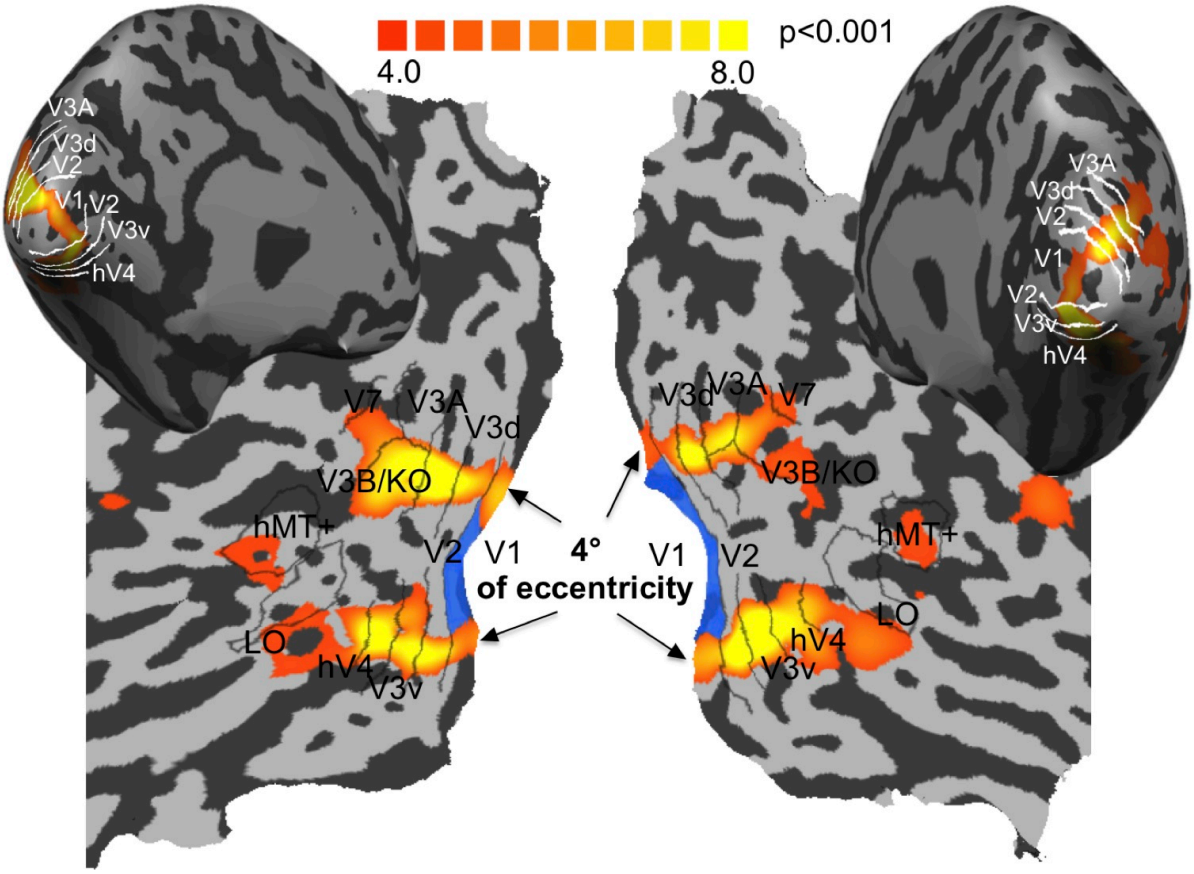

947

948

949 **Figure 7: ROIs delineation.**

950 Mapping of Regions of Interest (ROIs). We identified: 1) retinotopic areas, 2) the Lateral Occipital
951 complex (LO) and 3) motion-related areas (V3B/KO, hMT+/V5).). Functional activation (from red to
952 yellow, for low to high activation) from the braided control (4 deg eccentricity) versus fixation
953 conditions was projected onto each inflated or flattened hemisphere (Left: left hemisphere; Right: right
954 hemisphere for one subject). The blue shading in area V1 indicates the retinotopic regions interior to
955 the activation by the 4-degree eccentric contours of the control stimulus, based on the eccentricity
956 maps obtained from the retinotopy mapping experiment. This defines the region interior to the stimuli
957 from which the voxels were defined for the analyses in order to exclude voxels responding directly to
958 the contour.

959

960 **Tables**

961
962 **Table 1: Stimulus and response differences tested by classifiers.**
963

	Edge continuity	Interior chromaticity	Interior perceived color
Edge-dependent vs Control	**X**		**X**
Surface vs Control		**X**	**X**
Surface vs Edge-dependent	**X**	**X**	

964
965 The X's indicate the features on which the comparisons differed. The pattern of responses across the
966 three classifiers and not a single classification constrains the specificity of the region tested.

967

968 **Table 2: Post-hoc t-tests (Tukey Honest Significant Differences test) for differences of**
969 **classification accuracy between rules within areas.**

MVPA rule	I - II		I - III		II - III	
	t	p	*t*	p	*t*	p
Retinotopic areas						
V1	-2.50	**3.3e-02**	2.30	5.6e-02	4.80	**5.2e-06**
V2	-0.88	6.6e-01	1.30	3.9e-01	2.20	7.6e-02
Ventral visual areas						
V3v	-3.10	**6.6e-03**	-4.30	**6.4e-05**	2.20	6.9e-02
hV4	-4.70	**1.0e-05**	-2.50	**3.8e-02**	-2.30	2.2e-01
LO	-2.10	8.2e-02	-5.20	**9.3e-07**	-3.00	**7.5e-03**
Dorsal visual areas						
V3d	0.99	5.8e-01	-0.54	8.5e-01	-1.50	2.8e-01
V3A	6.50	**4.7e-10**	8.50	**4.0e-17**	2.10	1.0e-01
V7	-0.64	8.0e-01	1.40	3.3e-01	2.10	9.8e-02
V3B/KO	7.10	**9.5e-12**	7.30	**2.2e-12**	0.20	9.8e-01
hMT+/V5	0.35	9.3e-01	0.94	6.1e-01	0.59	8.2e-01

970

971 *Roman numerals refer to classification rules:* (I) Edge-dependent vs. control; (II) Surface-dependent
972 vs. control; (III) Surface-dependent vs. edge-dependent. Each column indicates the t- and p-values
973 for the difference of a pair of classification rules. Significance levels for $p < 0.05$ are indicated in bold.

974
975

Supplementary Figures

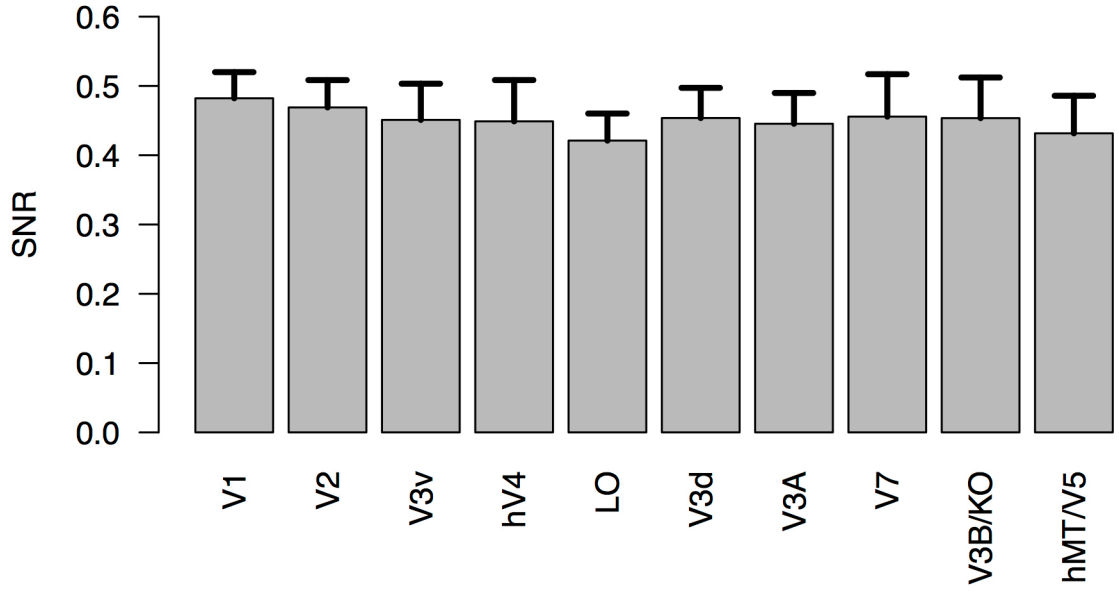

Figure S1: Functional signal-to-noise ratio (SNR) across all regions of interest (ROIs) for responses to stimuli in the main experiment.

Average functional signal-to-noise ratio was computed for the voxels included in the multivariate analysis by taking the difference between the mean response to the stimuli and the mean response to the fixation, divided by the SD of the mean across all stimulus conditions and fixation. Error bars indicate 95% confidence intervals.

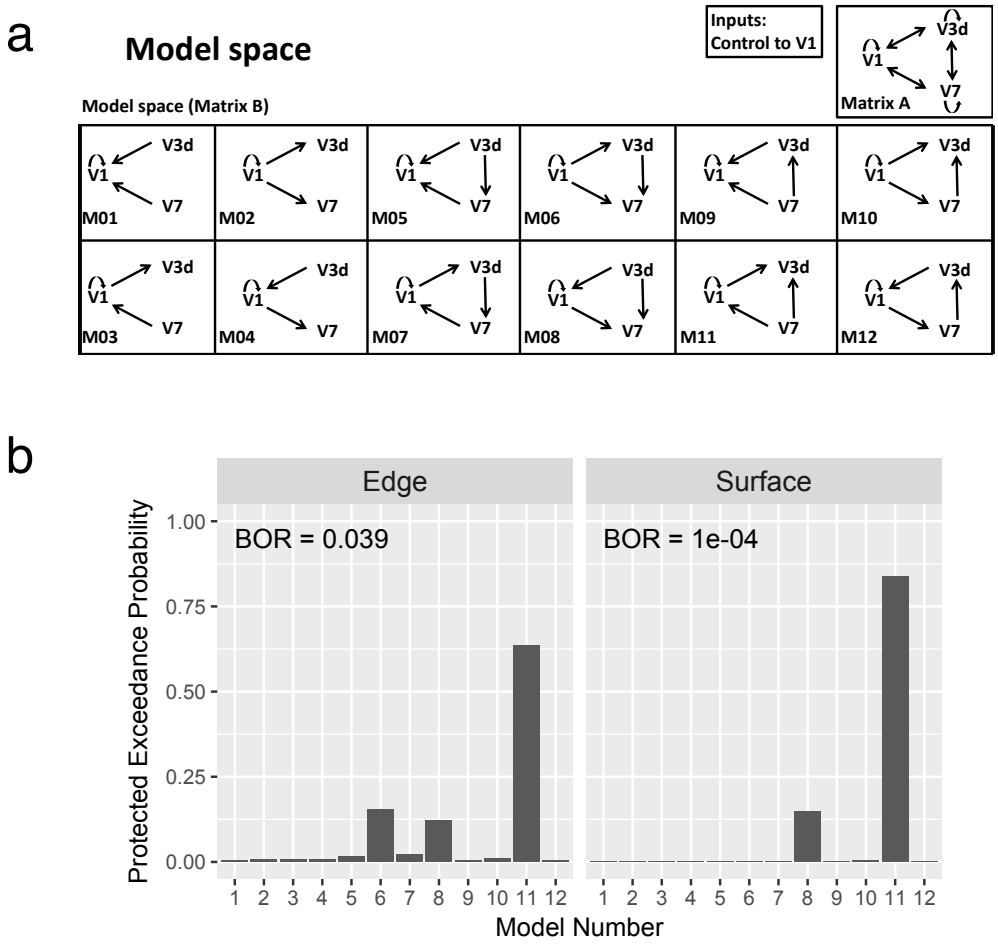

Figure S2: DCM Model space and protected exceedance probabilities for areas V1-V3d-V7. a) Twelve models (M0-M12) of the modulations of effective connectivities between areas V1, V3d and V7 were evaluated in the DCM analysis. The intrinsic connectivity (Matrix A) was taken to be complete within and between areas. Activations in response to the Control condition (braided stimuli, no perceived color) were used as input in V1, while activations in response to the Edge dependent or Surface dependent conditions could modulate effective connectivity (Matrix B) according to each model. Each model included self-modulation in V1 and unilateral modulations between V1 and area V3d and between V1 and area V7, yielding 4 possible combinations. Additionally there could either be no modulation between area V3d and area V7 (M01 to M04), unilateral modulation from area V3d to area V7 (M05 to M08) or unilateral modulation from area V7 to area V3d (M09 to M12). b) Protected exceedance probabilities (PEP) for each of the 12 models of modulation of the effective connectivities between the triple of areas indicated in (a) for the edge dependent (left) and surface dependent (right) stimuli. The Bayesian Omnibus Risk (BOR) is indicated in the upper left corner of each plot.

1002 **Supplementary Tables**

1003
1004 **Table S1: Average classification accuracy for each MVPA rule and ROI.**

MVPA rule	Edge-dependent vs. Control	Surface-dependent vs. Control	Surface-dependent vs. Edge-dependent
Retinotopic areas			
V1			
Multivariate	0.60 (0.006)	0.63 (0.008)	0.57 (0.009)
Shuffle	0.50 (0.009)	0.51 (0.007)	0.50 (0.010)
V2			
Multivariate	0.61 (0.008)	0.62 (0.012)	0.60 (0.010)
Shuffle	0.51 (0.009)	0.50 (0.009)	0.50 (0.010)
Ventral visual areas			
V3v			
Multivariate	0.58 (0.010)	0.62 (0.009)	0.64 (0.012)
Shuffle	0.50 (0.008)	0.51 (0.008)	0.51 (0.008)
hV4			
Multivariate	0.57 (0.010)	0.63 (0.012)	0.60 (0.012)
Shuffle	0.51 (0.007)	0.50 (0.010)	0.51 (0.007)
LO			
Multivariate	0.56 (0.009)	0.59 (0.011)	0.63 (0.013)
Shuffle	0.52 (0.008)	0.50 (0.008)	0.50 (0.006)
Dorsal visual areas			
V3d			
Multivariate	0.56 (0.009)	0.55 (0.013)	0.57 (0.011)
Shuffle	0.51 (0.008)	0.49 (0.009)	0.51 (0.009)
V3A			
Multivariate	0.68 (0.010)	0.59 (0.009)	0.56 (0.009)
Shuffle	0.51 (0.007)	0.50 (0.008)	0.50 (0.009)
V7			
Multivariate	0.55 (0.011)	0.56 (0.011)	0.53 (0.013)
Shuffle	0.51 (0.010)	0.50 (0.009)	0.51 (0.007)
V3B/KO			
Multivariate	0.64 (0.012)	0.55 (0.010)	0.55 (0.013)
Shuffle	0.51 (0.009)	0.51 (0.010)	0.49 (0.007)
hMT/V5			
Multivariate	0.56 (0.011)	0.56 (0.016)	0.55 (0.009)
Shuffle	0.52 (0.010)	0.51 (0.008)	0.51 (0.010)

1005

1006 Classification accuracies (N=16, mean and standard errors) for all tested areas. Columns: MVPA
1007 rules: edge-dependent (WCE) vs. control stimuli, surface-dependent vs. control stimuli, surface-
1008 dependent vs. edge-dependent (WCE) stimuli. Accuracies (standard errors) for multivariate analyses
1009 and shuffling analyses (i.e., with randomly assigned category labels, see Methods: *Control analyses*
1010 *for the MVPA*).
1011

1012 **Table S2: ANOVAs (F and p values) across MVPA rules and conditions for each area.**

	F	p	sig
Retinotopic areas			
V1			
Main effect of MVPA rules	16.58	1.4e-05	
Main effect of shuffled MVPA rules	0.14	0.87	ns
V2			
Main effect of MVPA rules	2.96	0.07	ns
Main effect of shuffled MVPA rules	1.19	0.32	ns
Ventral visual areas			
V3v			
Main effect of MVPA rules	7.61	2.12e-03	
Main effect of shuffled MVPA rules	0.30	0.74	ns
hV4			
Main effect of MVPA rules	11.78	1.67e-04	
Main effect of shuffled MVPA rules	0.93	0.40	ns
LO			
Main effect of MVPA rules	17.13	1.09e-05	
Main effect of shuffled MVPA rules	1.92	0.16	ns
Dorsal visual areas			
V3d			
Main effect of MVPA rules	0.87	0.42	ns
Main effect of shuffled MVPA rules	1.56	0.23	ns
V3A			
Main effect of MVPA rules	47.04	5.63e-10	
Main effect of shuffled MVPA rules	0.09	0.91	ns
V7			
Main effect of MVPA rules	1.53	0.23	ns
Main effect of shuffled MVPA rules	0.39	0.68	ns
V3B/KO			
Main effect of MVPA rules	27.27	1.78e-07	
Main effect of shuffled MVPA rules	1.65	0.21	ns
hMT+/V5			
Main effect of MVPA rules	0.28	0.76	ns
Main effect of shuffled MVPA rules	0.17	0.85	ns

1013

1014 F- and p-values for main effect of MVPA rule and shuffled MVPA rule in each ROI.

1015

1016
1017